Factors Influencing Dwell Fatigue Cracking in Notches of Powder Metallurgy Superalloys

T.P. Gabb, J. Telesman, and L. Ghosn
Glenn Research Center, Cleveland, Ohio

A. Garg
University of Toledo, Toledo, Ohio

J. Gayda
Glenn Research Center, Cleveland, Ohio

NASA STI Program . . . in Profile

Since its founding, NASA has been dedicated to the advancement of aeronautics and space science. The NASA Scientific and Technical Information (STI) program plays a key part in helping NASA maintain this important role.

The NASA STI Program operates under the auspices of the Agency Chief Information Officer. It collects, organizes, provides for archiving, and disseminates NASA's STI. The NASA STI program provides access to the NASA Aeronautics and Space Database and its public interface, the NASA Technical Reports Server, thus providing one of the largest collections of aeronautical and space science STI in the world. Results are published in both non-NASA channels and by NASA in the NASA STI Report Series, which includes the following report types:

- TECHNICAL PUBLICATION. Reports of completed research or a major significant phase of research that present the results of NASA programs and include extensive data or theoretical analysis. Includes compilations of significant scientific and technical data and information deemed to be of continuing reference value. NASA counterpart of peer-reviewed formal professional papers but has less stringent limitations on manuscript length and extent of graphic presentations.

- TECHNICAL MEMORANDUM. Scientific and technical findings that are preliminary or of specialized interest, e.g., quick release reports, working papers, and bibliographies that contain minimal annotation. Does not contain extensive analysis.

- CONTRACTOR REPORT. Scientific and technical findings by NASA-sponsored contractors and grantees.

- CONFERENCE PUBLICATION. Collected papers from scientific and technical conferences, symposia, seminars, or other meetings sponsored or cosponsored by NASA.

- SPECIAL PUBLICATION. Scientific, technical, or historical information from NASA programs, projects, and missions, often concerned with subjects having substantial public interest.

- TECHNICAL TRANSLATION. English-language translations of foreign scientific and technical material pertinent to NASA's mission.

Specialized services also include creating custom thesauri, building customized databases, organizing and publishing research results.

For more information about the NASA STI program, see the following:

- Access the NASA STI program home page at *http://www.sti.nasa.gov*

- E-mail your question via the Internet to *help@sti.nasa.gov*

- Fax your question to the NASA STI Help Desk at 443–757–5803

- Telephone the NASA STI Help Desk at 443–757–5802

- Write to:
  NASA Center for AeroSpace Information (CASI)
  7115 Standard Drive
  Hanover, MD 21076–1320

NASA/TM—2011-217118

Factors Influencing Dwell Fatigue Cracking in Notches of Powder Metallurgy Superalloys

T.P. Gabb, J. Telesman, and L. Ghosn
Glenn Research Center, Cleveland, Ohio

A. Garg
University of Toledo, Toledo, Ohio

J. Gayda
Glenn Research Center, Cleveland, Ohio

Acknowledgments

Level of Review: This material has been technically reviewed by technical management.

Available from

Factors Influencing Dwell Fatigue Cracking in Notches of Powder Metallurgy Superalloys

T.P. Gabb, J. Telesman, and L. Ghosn
National Aeronautics and Space Administration
Glenn Research Center
Cleveland, Ohio 44135

A. Garg
University of Toledo
Toledo, Ohio 43606

J. Gayda
National Aeronautics and Space Administration
Glenn Research Center
Cleveland, Ohio 44135

Abstract

The influences of heat treatment and cyclic dwells on the notch fatigue resistance of powder metallurgy disk superalloys were investigated for low solvus high refractory (LSHR) and ME3 disk alloys. Disks were processed to produce material conditions with varied microstructures and associated mechanical properties. Notched specimens were first subjected to baseline dwell fatigue cycles having a dwell at maximum load, as well as tensile, stress relaxation, creep rupture, and dwell fatigue crack growth tests at 704 °C. Several material heat treatments displayed a bimodal distribution of fatigue life with the lives varying by two orders-of-magnitude, while others had more consistent fatigue lives. This response was compared to other mechanical properties, in search of correlations. The wide scatter in baseline dwell fatigue life was observed only for material conditions resistant to stress relaxation. For selected materials and conditions, additional tests were then performed with the dwells shifted in part or in total to minimum tensile load. The tests performed with dwells at minimum load exhibited lower fatigue lives than max dwell tests, and also exhibited early crack initiation and a substantial increase in the number of initiation sites. These results could be explained in part by modeling evolution of peak stresses in the notch with continued dwell fatigue cycling. Fatigue-environment interactions were determined to limit life for the fatigue cycles with dwells.

Introduction

A new generation of powder metallurgy (PM) disk superalloys has been designed for higher engine operating temperatures by improvement of their strength and creep resistance. New PM disk superalloys have been designed with higher refractory element contents than cast and wrought superalloys, while avoiding segregation of chemistry and microstructure that are produced by cast and wrought processing (Refs. 1 and 2). Compared to cast and wrought superalloys, PM disk superalloy processing produces more uniform microstructures, with more consistent grain and precipitate size, and finer carbide sizes (Ref. 3). This processing also enables composition modifications designed to improve tensile, strength, and creep resistance, which allow disk applications at higher temperatures (Refs. 4, 5, and 6) in aerospace gas turbine engines.

However, the increased strength and creep resistance of these alloys may also increase the alloys notch sensitivity to fatigue loading and have a profound effect on the notched low cycle fatigue (NLCF) life (Ref. 7). Recent work has indicated that NLCF life for PM disk alloys is highly affected by sustained dwells at the higher disk operating temperatures (Ref. 8). It is therefore important to understand what

factors influence the resistance of PM superalloys to cracking at notches during fatigue cycling with load dwells.

The effect of prolonged high temperature dwells on low cycle fatigue and notched low cycle fatigue (LCF) behavior in this class of alloys is thought to be a product of complex interactions of cyclic loading damage, surface environmental degradation and embrittlement, as well as the visco-plastic material response to temperature and load history. Further, in superalloy gas turbine components, fatigue failures can often initiate at holes and other notched features. This is largely driven by the concentration of applied stresses and resulting damage due to the geometry of such features. But it can also be influenced by numerous other factors, including the effects of microstructure and associated mechanical properties of the superalloy. Additionally, the machining processes used to produce the notches could produce altered surface roughness, microstructural damage, and residual stresses that also could affect fatigue resistance (Ref. 7). Therefore, the effects of dwells on fatigue cracking at notches needs to be understood for these high temperature alloys.

The effect of dwells is known also to significantly affect the hold time crack growth behavior of the PM disk alloys. It has been shown recently (Ref. 9) that control of microstructural parameters by varying the cooling rates from the solution temperature, and also varying subsequent aging treatment has a profound effect on dwell crack growth behavior. The relationship between microstructural parameters and hold time crack growth has been linked to the effect of these parameters on stress relaxation behavior. The relationship between stress relaxation and notch dwell LCF behavior has not been explored and needs to be investigated due to the possibility of exhibiting similar relationship as has been identified in case of dwell crack growth.

The objective of this study was to investigate the effect of microstructure, environmental exposure and load history on notched LCF behavior of two advanced PM disk superalloys. The investigated microstructural parameters were grain size and precipitate size. Notched specimens were machined and fatigue tested with cycles incorporating dwells. Fatigue life and failure modes were characterized and related to microstructures and associated mechanical properties.

Materials and Procedure

P/M Processing

The two PM superalloys tested in the study were low solvus high refractory (LSHR) (Ref. 10) and ME3 (Refs. 11 to 14) alloys. Two versions of the LSHR alloy were tested. A "subscale LSHR" version was produced using a subscale atomizer by PCC Special Metals Corp., and passed through screens of –270 mesh (53 μm) mesh width to give powder particle diameters of no more than this size. The powder was then sealed in a stainless steel container, hot isostatic pressed, and extruded at a reduction ratio of 6:1. The extrusion billet was machined to segments about 9 cm in diameter and 20 cm long, which were isothermally forged into flat LSHR disks about 15 cm in diameter and 4 cm thick by PCC Wyman-Gordon Forgings.

An additional "production scale LSHR" version (Ref. 15) was also produced, using different powder processing procedures. This powder was produced in argon using a production-scale atomizer and handling procedures designed to minimize non-metallic inclusion content, by PCC Special Metals Corp. This powder was passed through –270 mesh screens, sealed in a container, hot compacted, and extruded at a reduction ratio of 6:1. A segment of the extrusion billet was machined to 15 cm diameter and 20 cm long, then isothermally forged into a larger flat disk than for the subscale material, about 30 cm in diameter and 5 cm thick. The measured compositions of both LSHR heats are listed in Table 1.

Specimens of another powder metallurgy disk superalloy, ME3 were also obtained. This powder was also produced in argon using production-scale atomization and handling procedures designed to minimize non-metallic inclusion content. This powder was passed through –270 mesh screens, then sealed in containers, hot compacted, and extruded at reduction ratios near 6:1. Extrusion segments were forged into

larger, contoured disks having diameters of about 61 cm and maximum thicknesses of about 5 cm. The average measured composition of ME3 alloy is also listed in Table 1.

Heat Treatments

To evaluate the influence of microstructural parameters on the mechanical properties, six heat treatments of the subscale atomized LSHR disks of 15 cm in diameter and 4 cm thick were performed to vary microstructure in this material, as described in Table 2. Four of the conditions used a subsolvus solution heat treatment to produce fine grain size, followed by either oil quenching (FGOQ) or fan cooling (FGFC) of the disks. Two of the conditions used a supersolvus heat treatment of 1171 °C for 1 h, then fan cooling of the disk (CGFC). The disks were then sliced in half, and halves were given either a one step aging heat treatment of 775 °C for 8 h or a two step aging heat treatment of 855 °C for 4 h + 775 °C for 8 h, to vary γ' size. The resulting six material conditions of subscale LSHR were therefore designated FGOQ1, FGOQ2, FGFC1, FGFC2, CGFC1, and CGFC2. The larger "production scale" LSHR disk was given a supersolvus heat treatment of 1171 °C for 1 h and fan cooled, then a single-step aging heat treatment of 855 °C for 8 h.

The ME3 disks were given a supersolvus heat treatment at 1171 °C for 1 h, fan plus oil quench, a stabilization heat treatment at 843 °C for 4 h, and an aging heat treatment of 760 °C for 8 h. The processing and properties of this material have been previously described and published elsewhere (Refs. 13 and 14).

Mechanical Testing

Tensile-stress relaxation, creep rupture, dwell fatigue crack growth, strain-controlled fatigue, and dwell notched fatigue tests were performed at 704 °C. Tensile-stress relaxation tests were performed on specimens having a gage diameter of 4 mm and gage length of 20 mm in a uniaxial test machine employing a resistance-heating furnace and axial extensometer. The tests were performed in general accordance with the tensile test specification ASTM E21, using an initial test segment with strain increased at a uniform rate of 0.5 percent per min. However, the tests were stopped at 1 percent strain and held for 100 h, to measure relaxation of stress as a function of time. The tensile tests were then continued to failure, at a faster uniform displacement rate of 1 mm per min., giving an approximate strain rate of 5 percent per min. across the gage length.

Combination uniform gage-notched creep rupture specimens (Fig. 1) having a notch elastic stress concentration factor $K_t = 2$ were machined for each LSHR condition. The notch was consistently low-stress ground, then polished parallel to the loading direction to meet or exceed a 0.21 μm (8 μin.) rms finish requirement. Six specimens were tested for each material condition at Metcut Research Associates in general accordance with creep test specification ASTM E139, using uniaxial lever arm creep testing machines with resistance-heating furnaces and extensometers attached to the uniform gage section. These creep-rupture tests were run at a constant load giving an initial applied stress of 793 MPa, interrupted at 0.5 percent strain to verify creep strain and elongation, then continued to failure at NASA GRC.

Fatigue crack growth specimens had a rectangular gage section 1 cm wide and 0.46 cm thick, with a surface flaw on one side of the gage section about 0.356 mm wide and 0.178 mm deep, produced by electro-discharge machining (Ref. 16). The fatigue crack growth specimens were then tested at NASA. Tests were performed in a closed-loop servo-hydraulic test machine using resistance heating, with potential drop measurement of crack growth. Pre-cracking was performed at room temperature, then tests were performed at elevated temperatures using a maximum stress of 620 MPa, stress ratio of 0.5, and dwell time of 90 s at maximum stress in each cycle.

Notched fatigue tests of LSHR were performed on cylindrical notched specimens (Fig. 1) having a geometric stress concentration factor $K_t = 2.0$. The notch was consistently low-stress ground, then polished parallel to the loading direction to a 0.21 μm (8 μin.) finish. Notched fatigue tests of ME3 were performed on slightly different cylindrical notched specimens (Fig. 1) having a geometric stress

concentration factor K_t of 2.0. Notch radius, diameter, and roughness were measured on all specimens before testing to insure consistency. All specimens were tested using uniaxial closed-loop servo-hydraulic testing machines with resistance heating furnaces at NASA GRC, in accordance with load-controlled fatigue test specification ASTM E466.

Six tests were performed for each material condition of subscale LSHR, with a baseline dwell fatigue cycle having 1 s loading ramps, dwell of 90 s at maximum net section stress (load/notch diameter) of 793 MPa, and minimum/maximum stress ratio ($R_\sigma = \sigma_{min}/\sigma_{max}$) of 0.05 in each cycle. Each test was continued to at least 2,000 cycles. At least two surviving specimens were continued to failure for each condition. Additional tests were performed on selected samples of subscale LSHR, full-scale LSHR, and ME3 using different cycle profiles (Fig. 2) with dwells at maximum ("maximum dwell") and minimum ("minimum dwell") tensile load, or combined dwells at both maximum and minimum load ("maximum-minimum dwells"), with maximum net section stresses of 793 or 855 MPa and $R_\sigma = 0.05$.

Several strain-controlled tests of ME3 were also performed on conventional fatigue specimens having a uniform cylindrical gage of 6.4 mm diameter and 19 mm length. These low cycle fatigue (LCF) specimens were tested using a uniaxial closed-loop servo-hydraulic testing machine with a resistance heating furnace and axial extensometer. The tests were performed according to strain-controlled fatigue test specification ASTM E606, with strain controlled to fixed limits. A triangular waveform was employed to vary strain at a frequency of 0.5 Hz over a total strain range of 1.0 percent at a strain ratio ($R_\varepsilon = \varepsilon_{min}/\varepsilon_{max}$) of 0. Dwells of 90 s were superimposed in each cycle at maximum or minimum strain.

Fractographic and Microstructural Evaluations

Fracture surfaces of fatigue specimens were evaluated by scanning electron microscopy (SEM). Crack initiation origins and crack propagation failure modes were identified and characterized. Metallographically-prepared sections from selected specimens were used to determine the grain sizes according to ASTM E112 linear intercept procedures using circular grid overlays, and as-large-as (ALA) grain sizes were determined using E930. Precipitate microstructures were compared using transmission electron microscopy (TEM) in dark field imaging conditions, of grains oriented with an <001> zone axis nearly perpendicular to the electrochemically-thinned foil. Statistical analyses of variance were performed using JMP (SAS Institute, Inc.) software, with significance assessed at a probability p = 0.05, representing 95 percent confidence.

Results and Discussion

Material Microstructures

The various heat treatments performed on the LSHR alloy did vary both grain size and the precipitate size, as listed in Table 2. Typical grain microstructures are shown in optical images from etched metallographic sections of test specimens in Figure 3. Subscale LSHR samples had mean intercept grain sizes near ASTM 12.4 (4.4 μm) for subsolvus heat treatment conditions, and ASTM 8.9 (14.5 μm) for supersolvus heat treatment conditions. Production-scale LSHR samples had a mean intercept grain size of 29 μm (ASTM 6.9). The ME3 production-scale samples had mean intercept grain sizes of 28 μm (ASTM 6.9).

TEM dark field images of subscale LSHR sections showing γ′ precipitates are compared in Figure 4 and detailed in Table 3. As shown, mean equivalent radius of mean secondary γ′ precipitates was larger for fan cooled than oil quenched fine grain disks, and coarse grain fan cooled disks had the largest mean size. Mean radius of tertiary γ′ precipitates increased in going from the single to two step aging heat treatments, while their numbers appeared to decrease. Images for production-scale LSHR and ME3 are also shown in Figure 4. Mean tertiary γ′ precipitate radius of production scale LSHR was similar to that of the subscale conditions having two-step aging heat treatments. Secondary γ′ precipitate size was larger

for the production scale LSHR, due to the larger disk size and slower corresponding cooling rate during fan cooling. ME3 had intermediate secondary and tertiary γ′ precipitate sizes.

Baseline Dwell Fatigue Resistance as a Function of Material Condition in Subscale LSHR

Fatigue Life

Fatigue life for the baseline dwell fatigue cycle is compared for the six different subscale LSHR material conditions studied, in Figure 5 (Ref. 10). Notch dwell fatigue testing of the first twelve specimens, two from each condition, produced interesting divergent results. Three of twelve failed in less than 500 cycles, while all others failed well over 10,000 cycles. Based on these results, the remaining 24 tests were run to 2,000 cycles to screen for more of the short life failures, having lives less than a 500 cycles.

All the short life failures were confined to two of the single-step aging heat treatments investigated, FGOQ1 and CGFC1. All specimens of these two material conditions were continued to failure, as well as those for the FGFC2 condition, to compare their distributions in lives. As seen in Table 4 and Figure 5, the population of failures was bimodal for the FGOQ1 and CGFC1 material conditions, with 7 of 12 specimens failing in less than 500 cycles and the remaining specimens reaching lives up to 100,000 cycles. Meanwhile, all failures for the FGFC2 condition were near 35,000 cycles.

Comparing the respective material conditions, it was evident that the wide scatter in life did not show a consistent dependence on solution heat treatment temperature and resulting grain size. The wide scatter was observed in conditions having fast and slow quench cooling rates. It was present for some, though not all conditions having a one step aging heat treatment, and absent for conditions having a two step aging heat treatment. Thus, conditions with wide scatter in fatigue life did not possess consistent corresponding heat treatment, grain size, or secondary γ′ size. Therefore, other factors were considered, focusing on what differences segregated the FGOQ1 and CGFC1 conditions, and could help explain their wide variations in notched dwell fatigue life.

Failure Initiation Modes

Typical failure initiation sites are shown in Figure 6. FESEM images from longitudinal sections are shown in Figure 7. Surface cracks initiated from grain boundaries or non-metallic inclusions along the notch root to cause failures for both short and long life tests for specimens of both FGOQ1 and CGFC1 conditions, as well as for the other material conditions. Examination of the notch surfaces adjacent to fatigue cracks and of metallographically-prepared longitudinal sections of failed specimens indicated multiple oxidized secondary cracks occurred along grain boundaries (Fig. 7), extending in from the notch surface for all material conditions. However, specimens having short lives did not display as many secondary cracks. The inclusions were usually alumina, either singular (Type 1) or granulated (Type 2) inclusions (Ref. 3). Their occurrence as crack initiation sites in some specimens having both long and short lives indicated they were not the singular cause of short lives, but were a complicating factor. After initiation, cracks predominantly grew along grain boundaries. Overall, it was clear that the wide scatter in life did not consistently correlate with a change of the predominant failure modes.

Examinations of the notch surfaces were conducted to determine whether the variability in the notch radius or surface roughness correlated with NLCF behavior. Specimen machining specifications for the notch permitted a tolerance and thereby variations in notch roughness as well as radius and associated stress concentration factor. However, notch radius and roughness had been measured, and found to be comparable for all material conditions. Radius and valley roughness (R_v) of the notches did not significantly correlate with fatigue life among specimens for the FGOQ1 and CGFC1 conditions, Figure 8. Hence, the wide scatter in lives could not be attributed to variations in notch roughness or radius. Cold work could also be qualitatively compared, by viewing distortion of the near-surface microstructure in longitudinal sections of several failed specimens. As shown in Figure 7, distortion of the near surface

microstructure was comparably small for both short and long life specimens of FGOQ1 and CGFC1 material conditions. However, these notches were too small and constricted for measuring residual stress in the loading direction by x-ray diffraction.

Correlations with Other Mechanical Properties

Fatigue crack growth tests with 90 s dwells at maximum stress were performed to assess the dwell fatigue crack growth behavior. Since the notch LCF life consists of both crack initiation and propagation portions, it was important to quantify the crack propagation to ascertain whether the differences in dwell crack growth could possibly explain the variation in NLCF lives. Fatigue crack growth rates are compared versus stress intensity factor in Figure 9. The six material conditions produced a range of 10x in crack growth rate response. The FGOQ1 condition exhibited the highest crack growth rates, while the CGFC2 condition had the slowest. However, the CGFC1 scatter condition had intermediate crack growth rates. Crack growth occurred by predominantly intergranular failure for all material conditions, Figure 10. So the FGOQ1 and CGFC1 conditions having wide scatter in life did not consistently have the highest crack growth rates, and had the same general intergranular failure mode as other conditions. Therefore, crack initiation rather than crack growth characteristics played a more significant role in explaining the wide scatter of notch dwell fatigue life.

Lives for constant load tests of combination uniform gage-notched creep rupture specimens, tested at the same stress as for the fatigue tests, are compared in Table 5 and Figure 11. The FGOQ1 and CGFC1 conditions did have highest 0.2 percent creep and rupture lives. However, only one specimen of the 36 tested failed at the notch, a CGFC1 specimen with a very short life of only 5.8 h. All other specimens failed in the uniform gage section at over 100 h. Single tests of notched specimens at the same notch section stress indicated notched rupture lives were at least usually twice those of the uniform gage tests. However, notch lives could be near or lower for the FGOQ1 and CGFC1 conditions. Associated rupture ductilities are also compared in Figure 11. The FGOQ1 and CGFC1 conditions had lowest rupture ductilities, while FGFC2 and CGFC2 conditions had highest values. Failure modes are compared in Figure 12. Intergranular surface cracks caused failures for all conditions. Hence, these rupture tests indicated the wide scatter in dwell fatigue life occurred for material conditions consistently having high monotonic creep resistance, and low rupture ductility.

Tensile yield and ultimate strengths are compared along with tensile ductility for the six LSHR conditions in Table 6 and Figure 13. The FGOQ1 and CGFC1 conditions had highest ultimate strengths of the six conditions. The FGOQ1 condition also had highest yield strength, while the CGFC1 condition intermediate yield strength. The CGFC2 condition had the lowest strength, but highest ductility. The FGOQ1 condition had lowest ductility of the six conditions, while the CGFC1 condition had intermediate ductility. As shown in Figure 14, small intergranular surface cracks initiated for all conditions, while microvoid coalescence occurred over much of the cross-section. Therefore, conditions giving the wide scatter in fatigue life did not consistently have the highest yield strength or lowest ductility, but did have consistently higher ultimate tensile strength.

These tensile tests had been interrupted at 1 percent strain, to measure stress relaxation as a function of time, shown in Figure 15. The FGOQ1 and CGFC1 conditions producing the bimodal life distribution in max dwell fatigue life were more resistant to stress relaxation than all other conditions, and maintained higher stresses with increased time. The FGFC2 and FGOQ2 conditions had the most stress relaxation. Prior work on LSHR has shown that stress relaxation resistance was correlated with tertiary γ' size (Ref. 9). Comparisons for the FGOQ1 and CGFC1 conditions suggest the tertiary γ' do have finer radius values of 0.0065 to 0.011 μm and higher contents of several percent, compared to those values for other tested conditions at the same grain size, Figure 4. Variations in this microstructural feature could therefore be responsible in part for the bimodal life response. However, Figure 4 shows the FGFC1 condition had fine tertiary γ' size comparable to that of FGOQ1 and CGFC1, due to their common single step aging heat treatment, yet it had no evidence of the bimodal life response in the present tests. Therefore, it may be more likely that the stress relaxation response itself is linked to this bimodal life

behavior, which can be influenced by various combinations of secondary and tertiary γ′ size and area fraction distributions within the material.

Summarizing the correlations with other mechanical properties, the FGOQ1 and CGFC1 conditions having wide scatter in notched max dwell fatigue lives had highest ultimate tensile strengths, highest creep and rupture lives, and highest stress relaxation resistances, yet lowest rupture ductilities. The combination of high stress relaxation resistance with low rupture ductility appeared important in explaining the bimodal fatigue life response.

Dwell Fatigue Resistance as a Function of Dwell Cycle Profile

Subscale, Fine Grain LSHR

To further examine how dwells influence fatigue life response, additional tests were performed on selected samples of LSHR to examine the effects of different cycle profiles on fatigue life. Samples of the FGFC2 condition, which displayed low scatter in baseline dwell fatigue life, were tested at the same maximum stress of 795 MPa using cycle profiles that varied the location of the dwells. Three additional NLCF load profiles were investigated: 1) tests performed with 90 s dwells occurring at the minimum load; 2) 90 s maximum hold followed by a 90 s minimum hold; and 3) 45 s maximum hold followed by a 45 s minimum hold.

The resulting NLCF fatigue lives and the associated load histories are compared in Figure 16. All six baseline dwell fatigue cycle tests were run to failure, and had shown to reduce life about 10x (90 percent) from cyclic tests run at the same maximum stress and stress ratio at a frequency of 10 Hz. Surprisingly, tests with 90 s dwells at minimum tensile stress had significantly lower lives, about 10x (90 percent) lower than that of the baseline dwell fatigue cycle. This significant reduction in life in comparison to the maximum dwell specimens also occurred for the two other wave forms in which minimum load holds were incorporated.

Failure initiation modes for these alternative cycles are compared for FGFC2 LSHR in Figures 17 and 18. A 90 s dwell at minimum stress resulted in a significant increase in crack initiations occurring along the notch root, compared to maximum dwell and maximum-minimum dwell cycles, Figure 17. The modes of crack initiation are compared in Figure 18. The 90 s minimum dwell activated an enhanced, transgranular failure initiation mode. The cracks appeared associated with sites of local, concentrated oxidation. These cracks initiated at numerous locations along the notch root, and transgranular cracks were also evident adjacent to the fracture surface, Figure 19. Tests with dwells at maximum stress or at both maximum and minimum stress often failed from cracks initiating at surface grain boundaries. However, some of these tests also had failure initiations at inclusions and pores near the notch root. These defects were related to the pilot-scale atomization process used to produce powder for this material, and were a common fatigue failure initiation site due to this material's fine grain size (Ref. 3).

The crack propagation failure mechanism in these specimens was predominantly intergranular for maximum dwell and maximum-minimum dwell tests. Conversely, cyclic no dwell and minimum dwell tests had more transgranular crack growth near the initiation points. However, this trend was complicated by failures initiating from inclusions that sometimes were located at a small distance below the notch surface. In all cycle profiles, cracks at these inclusions would grow in a predominantly transgranular mode, until the resulting circular crack intersected the notch surface. The environment then appeared to alter the crack growth mode, activating intergranular cracking for tests with any dwell time at maximum stress.

In general, creep-fatigue-environment interactions and damage are known to occur during dwell fatigue in superalloys (Refs. 17 and 18). Such damage could be expected in these disk superalloys tested in the notch fatigue test conditions evaluated. Imposition of a 90 s maximum dwell reduced the life by approximately an order-of-magnitude in comparison to the cyclic tests (Fig 16). This reduction of life could have been caused by either the creep, fatigue, environmental damage or an interaction of these mechanisms.

The use of both maximum and minimum dwell load histories allowed for separate evaluations of damage contributions for the test conditions studied. While the maximum dwell test could encourage creep, fatigue, and environmental interactions and damage, the minimum dwell test clearly eliminates creep damage at high applied stresses. Yet, cyclic life significantly decreased, not increased, by eliminating the creep damage. This indicated creep deformation was not limiting dwell cyclic life, and that fatigue-environment interactions and damage were predominantly limiting life in all of these dwell fatigue cycles for fine grain LSHR material condition.

Similar results were recently published for notched dwell fatigue tests of another fine grain powder metallurgy disk superalloy, RR1000 (Ref. 8). While tests of rectangular double-edge notched specimens at 650 °C with shorter 10 s dwells at maximum stress did not reduce mean life from that of no dwell cyclic tests, 10 s dwells at minimum stress reduced life nearly 10x (90 percent). Enhanced crack initiations were also observed for this minimum dwell cycle.

Production Scale, Coarse Grain LSHR

Additional LSHR material was then tested in a similar manner, to investigate the effects of altered powder processing, heat treatment, and resulting microstructure on this response. This material had been produced using production-scale powder atomization and handling procedures, carefully designed to minimize inclusion content (Ref. 19). The resulting forged disk was given a supersolvus solution heat treatment to produce a coarse grain size, which had been shown in prior work to be much less prone to inclusion-initiated fatigue failures than fine grain material (Ref. 20). This was intended to minimize the chances for any inclusion-initiated failures near the notch surface, which had complicated failure mode evaluations in subscale LSHR. This disk was fan cooled, and then given a single aging heat treatment at the high aging temperature of 855 °C, but for a longer time of 8 h (Ref. 15). This aging heat treatment was intended to determine if the results obtained for the CGFC2 condition in the baseline dwell fatigue tests could be further improved by altered ageing.

Testing again was performed with 90 s dwells at maximum stress, minimum tensile stress, or split between maximum and minimum stress. The NLCF fatigue results are compared in Figure 20. Again, cycles with partial or total dwell times at minimum stress had significantly lower lives, up to 10x (90 percent) below that of the baseline maximum dwell fatigue cycle. This indicated creep damage was not limiting maximum dwell cyclic life, and that fatigue-environment interactions and damage were apparently limiting life in all of these dwell fatigue cycles for both fine- and coarse-grain LSHR.

Failure initiation modes for the alternative dwell cycles are compared for this production scale, coarse grain LSHR in Figures 21 and 22. Cracks again initiated at numerous locations along the notch root for the minimum dwell cycle, both at and below the fracture surface, Figure 21. Fewer cracks initiated failure for cycles with dwells only at maximum stress or at both maximum and minimum stress. For this coarse grain LSHR material, minimum dwell tests again activated transgranular failure initiations at sites of local, concentrated oxidation, Figure 22. Subsequent crack propagation was predominantly transgranular. Maximum dwell tests again had intergranular surface crack initiations and crack growth, but without inclusion-initiated failures as observed in subscale LSHR. Maximum-minimum dwells had more transgranular surface crack initiations, which transitioned within 100 μm depth to intergranular crack growth.

Therefore, both fine- and coarse-grain materials displayed lower fatigue lives when subjected to cycle profiles containing dwells at minimum applied stress. Minimum dwells promoted a higher frequency of cracks initiating along the notch surface than for maximum dwells. The crack propagation failure mode for minimum dwell cycles was transgranular in nature. From these results, it appeared that fatigue-environment damage interactions that drove crack initiation to limit life for tests with dwells at minimum stress were not concentrated at grain boundaries. However, subsequent crack propagation was affected differently by cycle profile. Crack propagation became intergranular in the presence of dwells at maximum stress, as observed in numerous prior studies of dwell crack growth at high temperatures (Refs. 18, 19, 21, and 9). This intergranular crack propagation would be more rapid for maximum stress dwells than the transgranular crack propagation from minimum dwells, due to sustained times at high

dwell stresses which could drive crack growth. This could help explain the lower lives observed for maximum-minimum dwell tests than for minimum dwell tests, for both fine- and coarse-grain LSHR.

Production Scale, Coarse Grain ME3

Notched fatigue specimens from another disk superalloy, ME3 (Refs. 11 and 12), were also obtained from larger, contoured disks. This material had been produced using production-scale powder atomization, handling, consolidation, forging, and supersolvus solution heat treatment procedures giving a coarse grain size (Ref. 13).

The effects of cycle profiles having 90 s dwells on fatigue life of ME3 were again assessed at 704 °C, using load cycles with a ramp of 1.5 s and $R_\sigma = 0.05$, but at a higher maximum stress of 855 MPa. The effects of maximum and minimum stress dwell cycles on life are shown in Figure 23. Lives at this higher stress level were lower than for LSHR, and maximum stress dwells reduced mean fatigue life by about 4x (75 percent) from 0.5 Hz cyclic tests. However, minimum stress dwells again further reduced mean fatigue life, giving 10x (90 percent) reduction in mean life from 0.5 Hz cyclic tests.

Unlike LSHR, mostly intergranular failure initiations were observed for ME3 under all dwell test conditions, Figure 24. For 90 s minimum dwell tests, three out of the four specimens tested exhibited intergranular initiation, with the fourth specimen exhibiting transgranular initiation. Relatively few failure initiation sites were present for cyclic no-dwell and maximum dwell tests. However, many failure initiation sites were observed along the notch surface for minimum dwell tests. Transgranular propagation was apparent for cyclic and minimum dwell, but intergranular crack propagation was observed following maximum stress dwell tests. This suggested the tensile load ramp was responsible for crack propagation in the minimum stress dwell test.

To determine the early stages of the crack initiation failure mode, an interrupted minimum dwell test was performed. The test was stopped periodically with the specimen placed in the SEM to determine the onset of cracking and the subsequent damage mechanisms. As shown in Figure 25, surface intergranular cracks initiated very early, and were present within the first 10 percent of fatigue life. Additional intergranular cracks initiated throughout the test. With continued cycling, cracks grew and were often linked.

The difference in failure initiation modes observed for minimum dwells in coarse grain ME3 and LSHR could be related to the higher stress of 855 MPa applied to ME3, in comparison to 793 MPa maximum stress applied to LSHR specimens. ME3 and LSHR did have comparable crack propagation mode response for varied cycle profiles. For both alloys, cyclic no-dwell and minimum dwell tests exhibited transgranular crack propagation, while cycles with dwells at maximum stress propagated by an intergranular crack propagation mechanism.

Strain-Controlled Tests of ME3

Cyclic dwell testing was conducted on uniform gage ME3 specimens to ascertain stress relaxation behavior under both maximum and minimum dwell conditions. The testing had total strain controlled using cyclic waveforms having no dwells, 90 s dwells at maximum tensile strain, or 90 s dwells at minimum tensile strain. These tests were intended to aid understanding of how fatigue response is affected by dwells in a notch, where the plastic zone at the root of a notch is constrained by the mostly elastic surrounding material, to constrain notch strains (Ref. 22).

Maximum and minimum stress for the strain-controlled tests as a function of cycles is compared for tests at 1.0 percent strain range in Figure 26. Tests with maximum strain dwells exhibited stress relaxation during each dwell, and both maximum and minimum stresses rapidly moved down in stress. Maximum stress was reduced by 20 percent after 200 cycles. Tests with minimum strain dwells had sustained maximum and minimum stresses, and remained relatively unchanged after 1,000 cycles. In similar tests of a prior study of ME3 at a lower 0.7 percent strain range (Ref. 23), which were continued to failure, the peak tensile cyclic stress in the maximum dwell test was reduced in a similar manner, which explained its very long life of about 100,000 cycles. In contrast, the corresponding min strain dwell cycle tests did not

show any significant stress relaxation, which resulted in considerably lower fatigue life of about 20,000 cycles, Figure 27. These collective results indicated dwells at minimum strains maintained higher peak stresses, which produced lower fatigue lives than for dwells at maximum strains. Similar effects would be expected in notches. However, effects of the stress concentration in a notch still had to be considered, using finite element modeling.

Finite Element Modeling of Stress Evolution in Notch of ME3

Finite element modeling was performed to model the notch dwell low cycle fatigue behavior of ME3 in an attempt to explain the unexpected behavior of the minimum dwells producing larger LCF life debit than maximum dwell tests. Two-dimensional axisymmetric finite element elastic-visco-plastic models were generated for the notched specimen. Stress-strain tensile data from uniform gage monotonic tensile-stress relaxation tests was used to model visco-plastic behavior in the notch specimens, and monotonic tensile stress-time relaxation data was used to model stress relaxation during the 90 s dwells for the notch.

Estimated maximum axial stresses generated at the notch root for ME3 specimens are compared as a function of maximum and minimum dwell cycles in Figure 28. As shown, tests with max dwells exhibited substantial stress relaxation during the maximum dwells, with the highest rate of stress relaxation occurring during the initial cycles. In comparison for the minimum dwell tests, the maximum stress remained almost constant throughout duration of the test. These analytical results were consistent with results of the strain-controlled tests of ME3, but now also estimated the effects of notches on local, concentrated stresses near the notch. These results indicated the minimum dwell cycle maintained higher peak stresses at the notch root than the maximum dwell cycle for which the high stresses only lasted in the first few cycles. Thus if the cracking did not initiate in the first few cycles of the maximum dwell NLCF test it is plausible that the subsequent reduction in the maximum stress during the dwells hindered the initiation and resulted in longer NLCF lives. In contrast, it is suspected that the high maximum stresses of the minimum dwell tests caused earlier initiations and led to lower NLCF lives.

Effect of Environment

The argument that the enhanced stress relaxation of the stresses during the maximum holds may explain the longer lives of the maximum dwell tests in comparison to the minimum dwells, but still does not account for the substantially larger number of cycles-to-failure observed in the no-dwell specimens in comparison to the minimum dwell specimens. The cyclic stresses estimated at the notch root for ME3 in minimum dwell and no-dwell fatigue tests at the same applied loads are compared in Figure 29. Maximum and minimum stresses at the notch root were sustained, and quite comparable for these two cases with continued cycling. However, the minimum dwell cycle produced significantly lower cyclic life than the no-dwell cycle.

This illustrated the strong effect of environment on fatigue life under these conditions. This signifies that fatigue-environment interactions and damage during dwells can severely limit notch fatigue life in the various dwell fatigue cycles performed here on fine grain LSHR, coarse grain LSHR, and coarse grain ME3, after accounting for stress evolution at the notch.

However, tests at higher temperatures and stresses could also activate other failure modes such as net-section creep rupture, while tests at lower temperatures could activate failure modes such as grain facet failures. Therefore, additional dwell fatigue testing and characterization would be necessary before extrapolating the present results to other test conditions.

Additional Work

Additional finite element modeling could be performed to estimate the maximum axial stresses generated at the notch root as a function of maximum dwell cycles for the FGOQ1 and FGFC2 conditions of subscale LSHR. The difference in monotonic stress relaxation at the notch root for the FGFC2 and FGOQ1 heat treatments could be reflected in cyclic stress relaxation rates. This could help explain the

different notched LCF behaviors for these two heat treatments, where the FGOQ1 heat treatment showed a bimodal distribution of dwell NLCF lives with half of the specimens failing within few hundred cycles, and the other half exhibiting two orders of magnitude longer lives. The lives of the FGFC2 specimens did not show this type of behavior with all the tested specimens exhibiting lives greater than 10,000 cycles.

Additional damage characterization work could help to increase understanding and enable modeling the effects of dwells on notched fatigue life. Careful longitudinal sectioning of secondary cracks in failed specimens, by metallographic preparation and other microscopy, could be used to examine multiple secondary fatigue cracks at various stages of formation and growth, to explain how the cracks initiate and grow. For the current materials and test conditions, additional interrupted testing could then be performed using various cycle profiles to quantify exactly how much crack initiation life is reduced by dwells, and what fatigue-environment damage feature is first to fail. With this knowledge a critical parameter of the damage feature could be derived, such as size necessary for failure, and how this parameter varies with time and cycles. Tests at other stresses and temperatures would provide the data to determine how this critical parameter varies with stress and temperature, and where other failure modes may emerge. Tests could also be performed using more complicated cycle profiles, which more closely simulate the dwell and cyclic segments of service cycles for aerospace gas turbine engines. These cycle profiles could eventually incorporate the temperature variations that occur in turbine engine cycles. Specimens with larger notches having open access could be designed and tested to allow measurements of residual stress and plasticity in the loading direction by x-ray diffraction both after machining and after interrupted fatigue testing.

This information could then be used as input for a fatigue life prediction model. The time and cycle-dependent growth of the life-limiting damage features could be modeled, as a function of notch geometry, surface residual stress and plasticity, cycle profile, applied stress and temperature.

Using these tools, strategies for improving dwell notched fatigue life could then be designed for experimentation. Heat treatments, machining, and final surface treatments could be modified to lower the stresses generated in notches that drive crack initiation and growth, for example by modifying yield strength and enhancing stress relaxation. Superalloy composition could possibly be modified to hinder formation of the critical fatigue-environment damage features. Alternatively, surface composition modifications or fatigue-resistant environmental barrier coatings could be evaluated.

However, potentially enhanced dwell notch fatigue cracking properties would need to be balanced with many other mechanical properties of importance for mechanical design of disks. This would include monotonic strength and creep resistance, as well as cyclic fatigue crack initiation and growth properties, at both uniform and notched locations.

Summary and Conclusions

The influences of heat treatment conditions and cycle profile on the notch fatigue resistance of powder metallurgy disk superalloys were investigated in both fine- and coarse-grain LSHR alloy and in a coarse-grain ME3 alloy. Several heat treatment conditions resulted in bimodal life distributions in baseline maximum dwell fatigue life, while others had more consistent fatigue lives. The bimodal distribution was characterized by some specimens failing within few hundred cycles, and others lasting two orders-of-magnitude longer. The bimodal failure distribution in baseline notch dwell fatigue life was present for only the heat treated material conditions that were resistant to stress relaxation and had high strength and low rupture ductility.

Shifting of the dwells from maximum load to minimum load substantially lowered NLCF life for both alloys at the tested material conditions. Minimun dwells promoted both early crack initiation and exhibited much greater number of crack initiation sites. The results pointed to a strong fatigue-environment interaction causing material damage which limited dwell fatigue life for all dwell test conditions studied. These results could be explained by considering the evolution of peak stresses in the notch with continued dwell fatigue cycling, and indicated dwell fatigue life in notches was limited by an interaction of fatigue and environmental damage.

It can be concluded from this work that:

1) Dwells reduce fatigue life in notches largely through fatigue-environment damage interactions, for these fine- and coarse-grain superalloy materials and test conditions.

2) The effects of dwells in reducing fatigue life at high temperatures can be influenced by varying cycle profiles; profiles and service cycles having dwells near minimum load can more severely reduce life.

3) Testing and modeling indicate this can be due to different evolutions of cyclic stresses in notches during dwell cycles, dependent on the dwell cycle profiles as well as the materials' stress-strain and stress relaxation responses.

4) Wide scatter can be observed in dwell fatigue life for materials having high strength, creep, and stress relaxation resistance subjected to dwells at maximum load. This can be due to both the limited stress-relaxation of cyclic peak stresses which these creep resistant heat treatments exhibit as well as their low and variable rupture ductility. Combination of these two characteristics can result in pre-mature intergranular cracking or rupture leading to a low life NLCF test result.

5) Dwell fatigue life is strongly influenced by the interaction of cyclic stresses in notches and environmental attack processes, so both aspects should be considered in modeling and prediction of fatigue life.

References

1. C.T. Sims, N.S. Stoloff, W.C. Hagel, Superalloys II, John Wiley & Sons, New York, NY, 1987, p. 477.
2. R.C. Reed, The Superalloys, Cambridge University Press, Cambridge, U.K., 2006, p. 242.
3. D.R. Chang, D.D. Krueger, R.A. Sprague, "Superalloy Powder Processing, Properties, and Turbine Disk Applications," Superalloys 1984, ed. M. Gell, C.S. Kortovich, R.H. Bricknell, W.B. Kent, J.F. Radavich, The Minerals, Metals & Materials Society, Warrendale, PA, 1984, pp. 245–252.
4. J.J. Schirra, S.H. Goetschius, "Development of an Analytical Model Predicting Microstructure and Properties Resulting From the Thermal Processing of a Wrought Powder Nickel-base Superalloy Component," Superalloys 1992, ed. S.D. Antolovich, R.QW. Stusrud, R.A. MacKay, D.L. Anton, T.Khan, R.D. Kissinger, D.L. Klarstrom, The Minerals, Metals & Materials Society, Warrendale, PA, 1992, pp. 437–446.
5. D.D. Krueger, R.D. Kissinger, R.G. Menzies, "Development and Introduction of a Damage Tolerant High Temperature Nickel-Base Disk Alloy, Rene′ 88DT, Superalloys 1992, ed. S.D. Antolovich, R.QW. Stusrud, R.A. MacKay, D.L. Anton, T. Khan, R.D. Kissinger, D.L. Klarstrom, The Minerals, Metals & Materials Society, Warrendale, PA, 1992, pp. 277–286.
6. D. Rice, P. Kantzos, B. Hann, J. Neumann, and R. Helmink , "P/M Alloy 10 - A 700°C Capable Nickel-Based Superalloy for Turbine Disk Applications," Superalloys 2008, ed. R.C. Reed, K.A. Green, P. Caron, T.P. Gabb, M.G. Fahrmann, E S. Huron. S.A. Woodard, The Minerals, Metals & Materials Society, Warrendale, PA, 2008, pp. 139–148.
7. D. Grieving, M. Gorelik, H. Kington, "Manufacturing Related Residual Stresses and Turbine Disk Life Prediction," Rev. of Quantitative Nondestructive Evaluation, CP760, V. 24, American Institute of Physics, 2005, pp. 1339–1346.
8. M.R. Bache, J.P. Jones, G.L. Drew, M.C. Hardy, N. Fox, "Environment and Time Dependent Effects on the Fatigue Response of an Advanced Nickel Base Superalloy," Int. J. Fatigue, V. 31, 2009, pp. 1719–1723.
9. J. Telesman, T.P. Gabb, A. Garg, P. Bonacuse, J. Gayda, "Effect of Microstructure on Time Dependent Fatigue Crack Growth Behavior in a P/M Turbine Disk Alloy," Superalloys 2008, ed. R.C. Reed, K.A. Green, P. Caron, T.P. Gabb, M.G. Fahrmann, E.S. Huron. S.A. Woodard, The Minerals, Metals & Materials Society, Warrendale, PA, 2008, pp. 807–816.
10. J. Gayda, T.P. Gabb, J. Telesman, "Notch Fatigue Strength of a PM Disk Superalloy," NASA/TM— 2007-215046, Washington, D.C., October, 2007.

11. D.P. Mourer, J.L. Williams, "Dual Heat Treat Process Development for Advanced Disk Applications," Superalloys 2004, ed. K.A. Green, H. Harada, T.E. Howson, T.M. Pollock, R.C. Reed, J.J. Schirra, S. Walston, The Minerals, Metals & Materials Society, Warrendale, PA, 2004, pp. 401–408.

12. J.R. Groh, D.P. Mourer, "Alternate Material for Elevated Temperature Turbine Cooling Plate Applications," Superalloys 2004, ed. K.A. Green, H. Harada, T.E. Howson, T.M. Pollock, R.C. Reed, J.J. Schirra, S. Walston, The Minerals, Metals, & Materials Society, 2004, pp. 101–108.

13. T.P. Gabb, A. Garg, D.L. Ellis, K.M. O'Connor, "Detailed Microstructural Characterization of the Disk Alloy ME3," NASA/TM—2004-213066, Washington, D.C., May, 2004.

14. T.P. Gabb, J. Telesman, P.T. Kantzos, A. Garg, "Effects of Temperature on Failure Modes for a Nickel-Base Superalloy," J. of Failure Analysis and Prevention, V. 7(1), 2007, pp. 56–65.

15. T.P. Gabb, J. Gayda, "Tensile and Creep Property Evaluations of Potential Brayton Impeller and Duct Materials," NASA/TM—2006-214110, Washington, D.C., February, 2006.

16. R.H. Vanstone, T.L. Richardson, "Potential-Drop Monitoring of Cracks in Surface-Flawed Specimens," ASTM STP 877, American Society for Testing and Materials, W. Conshohocken, PA, 1985, pp. 148–166.

17. S.S. Manson, G.R. Halford, M.H. Hirschberg, "Creep-Fatigue Analysis by Strain-Range Partitioning," Symposium on Design for Elevated Temperature Environments, American Society of Mechanical Engineers, New York, NY, 1971, pp. 12–28.

18. R.V. Miner, J. Gayda, R.D. Maier, "Fatigue and Creep-Fatigue Deformation of Several Nickel-base Superalloys at 650°C," Met. Trans. A, V. 13A, 1982, pp. 1755–1765.

19. A. Banik, K.A. Green, "The Mechanical Property Response of Turbine Disks Produced Using Advanced PM Processing Techniques," Superalloys 2000, ed. T.M. Pollock, R.D. Kissinger, R.R. Bowman, The Minerals, Metals & Materials Society, Warrendale, PA, 2000, pp. 69–74

20. T.P. Gabb, J. Gayda, J. Telesman, P. Kantzos, "Thermal and Mechanical Characterization of Disk Alloy LSHR," NASA/TM—2005-213645, Washington, D.C., June, 2005.

21. K.R. Bain, M.L. Gambone, J.M. Hyzak, M.C. Thomas, "Development of Damage Tolerant Microstructures in Udimet 720," Superalloys 1988, ed. D.N. Duhl, G. Maurer, S. Antolovich, C. Lund, S. Reichman, The Minerals, Metals & Materials Society, Warrendale, PA, 1988, pp. 13–22.

22. S.S. Manson, G.R. Halford, Fatigue and Durability of Structural Materials, ASM International, Metals Park, OH, 2006, p. 84.

23. T.P. Gabb, J. Telesman, P.T. Kantzos, J.W. Smith, "Effects of High Temperature Exposures on Fatigue Life of Disk Superalloys," Superalloys 2004, ed. K.A. Green, H. Harada, T.E. Howson, T.M. Pollock, R.C. Reed, J.J. Schirra, S. Walston, The Minerals, Metals & Materials Society, Warrendale, PA, 2004, pp. 269–274.

TABLE 1.—ALLOY COMPOSITIONS IN WEIGHT PERCENT

Wt. %	Al	B	C	Co	Cr	Mn	Mo	Nb	Ta	Ti	V	W	Zr	Ni
Subscale LSHR	3.60	0.02	0.03	20.5	12.4	0.09	2.8	1.5	1.2	3.50	0.1	4.3	0.05	Bal.
Prod. scale LSHR	3.70	0.03	0.03	20.8	12.6	0	2.44	1.4	1.64	3.49	0	4.3	0.05	Bal.
ME3	3.31	0.03	0.06	20.6	12.8	0	3.85	0.9	2.3	3.54	0	2.01	0.05	Bal.

TABLE 2.—HEAT TREATMENTS OF THE DIFFERENT MATERIALS

Material condition	Solution step	Quench	Age
LSHR FGOQ1	1135 °C / 1.5 h	Oil	775 °C / 8 h
LSHR FGOQ2	1135 °C / 1.5 h	Oil	855°C / 4 h + 775 °C / 8 h
LSHR FGFC1	1135 °C / 1.5 h	Fan air	775 °C / 8 h
LSHR FGFC2	1135 °C / 1.5 h	Fan air	855 °C / 4 h + 775 °C / 8 h
LSHR CGFC1	1171 °C / 1.5 h	Fan air	775 °C / 8 h
LSHR CGFC2	1171 °C / 1.5 h	Fan air	855 °C / 4 h + 775 °C / 8 h
Prod. scale LSHR	1171 °C / 1.5 h	Fan air	855 °C / 8 h
ME3	1171 °C / 1 h	Fan air + oil	843 °C / 4 h + 760 °C / 8 h

TABLE 3.—TYPICAL GRAIN SIZE AND γ' PRECIPITATE SIZES:
MEAN VALUE ± ONE STANDARD DEVIATION.

Material condition	Mean linear intercept grain size no.	Equivalent grain size, μm	Mean secondary γ' radius, μm	Mean tertiary γ' radius, μm
LSHR FGOQ1	12.5 ± 1.1	4.2	0.085 ± 0.016	0.0107 ± 0.0035
LSHR FGOQ2	12.3 ± 1.1	4.6	0.085 ± 0.021	0.0169 ± 0.0049
LSHR FGFC1	12.4 ± 1.1	4.3	0.089 ± 0.019	0.0118 ± 0.0048
LSHR FGFC2	12.5 ± 1.0	4.2	0.088 ± 0.024	0.0160 ± 0.0036
LSHR CGFC1	8.9 ± 1.8	14.7	0.122 ± 0.025	0.0065 ± 0.0031
LSHR CGFC2	8.9 ± 1.7	14.4	0.137 ± 0.031	0.0151 ± 0.0035
Prod. scale LSHR	6.9 ± 1.9	29	0.172 ± 0.058	0.0156 ± 0.0043
ME3 (Ref. 13)	6.9 ± 0.3	29	0.097 ± 0.021	0.0133 ± 0.0034

TABLE 4.—SUBSCALE LSHR CREEP RUPTURE RESULTS AT 704 °C/793 MPa:
MEAN VALUE ± ONE STANDARD DEVIATION (NUMBER OF TESTS).

Condition	0.2% creep, h	Gage rupture, h	Elongation, %	Notch rupture, h
FGOQ1	114.5 ± 20.5 (2)	333.7 ± 74.8 (6)	8.9 ± 2.0 (6)	400.7 (1)
FGOQ2	16.7 ± 1.3 (2)	135.1 ± 16.7 (6)	11.6 ± 2.0 (6)	425.3 (1)
FGFC1	79.2 ± 18.2 (2)	271.4 ± 37.4 (6)	12.6 ± 2.9 (6)	569.5 (1)
FGFC2	8.8 ± 0.9 (2)	127.2 ± 10.3 (6)	14.5 ± 1.5 (6)	563.0 (1)
CGFC1	104 (1)	387.4 ± 34.8 (5)	10.1 ± 5.4 (5)	5.8, 3687.9 (2)
CGFC2	16.4 ± 1.0 (2)	327.1 ± 80.1 (6)	13.1 ± 6.3 (6)	2273.0 (1)

TABLE 5.—TENSILE PROPERTIES AT 704 °C: MEAN VALUE ± ONE
STANDARD DEVIATION (NUMBER OF TESTS)

Material condition	0.2% yield strength, MPa	Ultimate strength, MPa	Elongation, %	Reduction in area, %
LSHR FGOQ1	1190 ± 26 (2)	1388 ± 23 (2)	7.3 ± 1.1 (2)	12.1 ± 3.6 (2)
LSHR FGOQ2	1168 ± 4 (2)	1329 ± 3 (2)	9.3 ± 0.5 (2)	14.6 ± 0.5 (2)
LSHR FGFC1	1129 ± 8 (2)	1327 ± 15 (2)	8.3 ± 1.8 (2)	12.7 ± 2.4 (2)
LSHR FGFC2	1117 ± 10 (2)	1296 ± 19 (2)	10.7 ± 2.4 (2)	18.3 ± 4.6 (2)
LSHR CGFC1	1073 ± 6 (2)	1367 ± 12 (2)	13.7 ± 0.9 (2)	18.4 ± 3.4 (2)
LSHR CGFC2	1029 ± 3 (2)	1334 ± 24 (2)	18.0 ± 1.4 (2)	29.6 ± 4.8 (2)
Prod. Scale LSHR	993 ± 59 (4)	1335 ± 48 (4)	17.2 ± 6.1 (4)	23.2 ± 9.5 (4)
ME3 (Ref. 13)	1007 ± 49 (2)	1303 ± 39 (2)	18.5 ± 3.1 (2)	22.5 ± 8.8 (2)
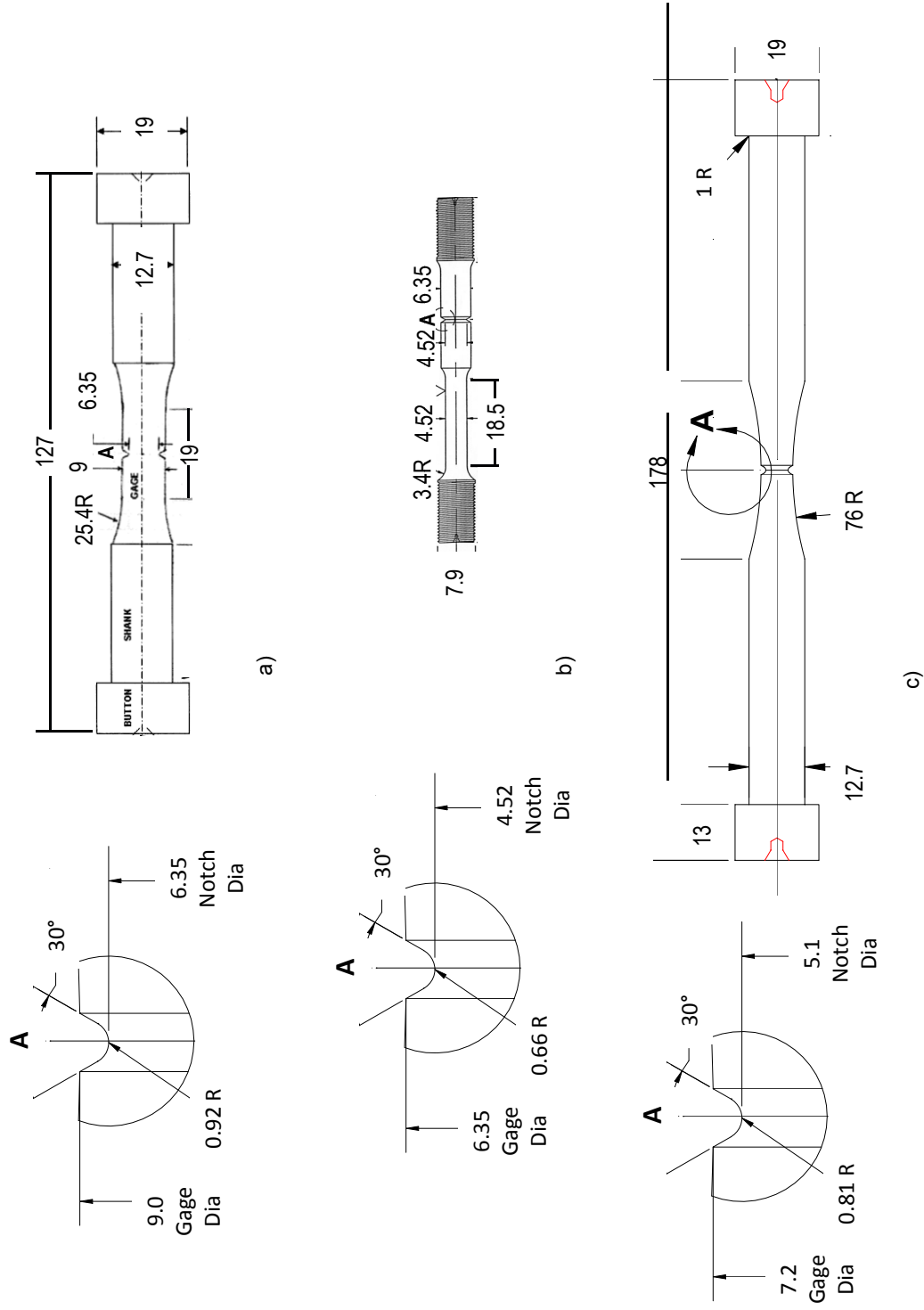
Figure 1.—Notched test specimens, with dimensions in millimeters; a) LSHR notched creep-rupture specimen; b) LSHR notched fatigue specimen; and c) ME3 notched fatigue specimen.
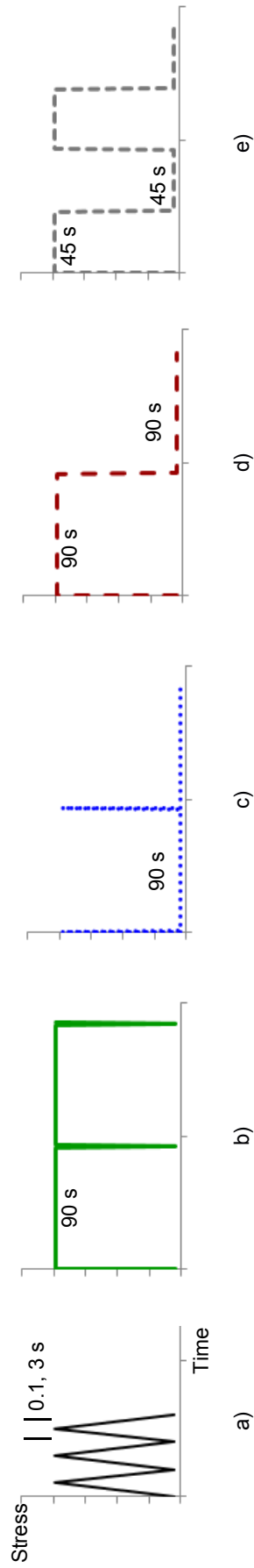
Figure 2.—Cycle profiles used in fatigue tests; a) No dwell, 0.5 and 10 Hz; b) 90 s dwell at maximum load ("maximum dwell"); c) 90 s dwell at maximum load ("minimum dwell"); d) 90 s dwell at maximum and minimum loads; and e) 45 s dwells at maximum and minimum loads.

CGFC1

CGFC2

FGFC1

FCFC2

FGOQ1

FGOQ2

a)

ME3

LSHR

b)
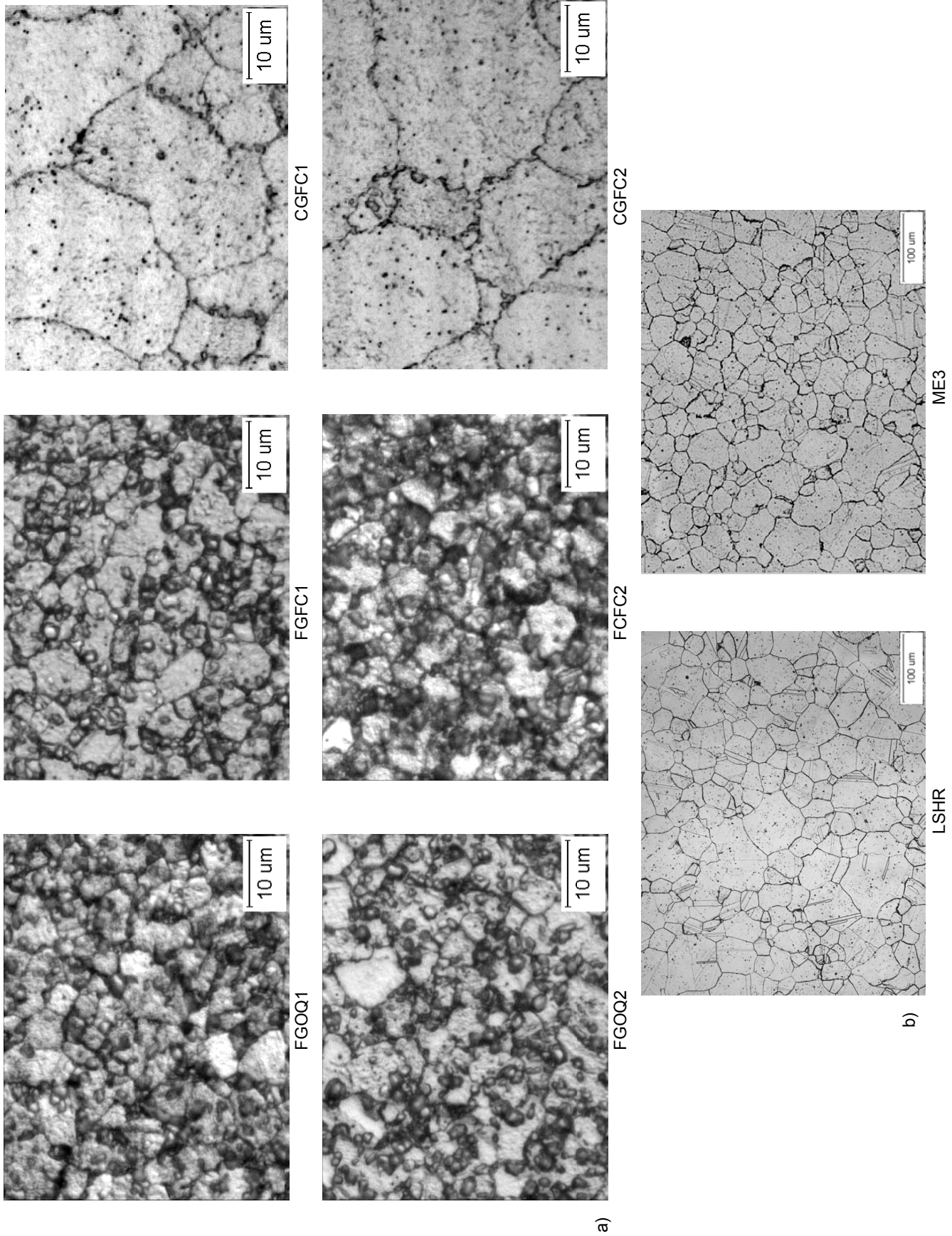
Figure 3.—a) Grain structure for the six conditions of subscale LSHR; and b) Grain structure for production scale LSHR and ME3.
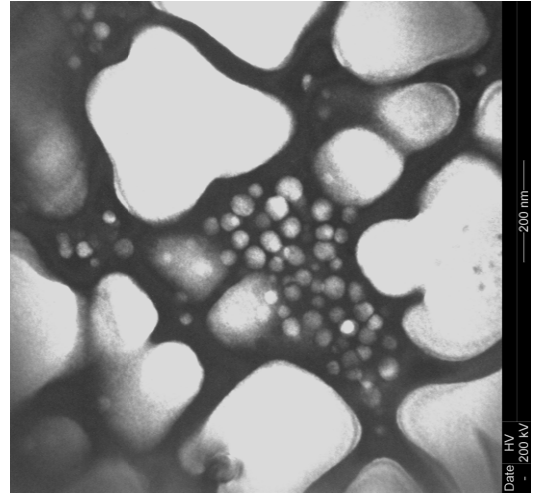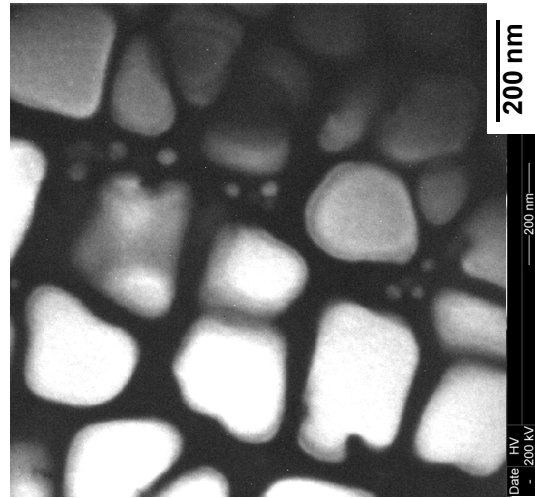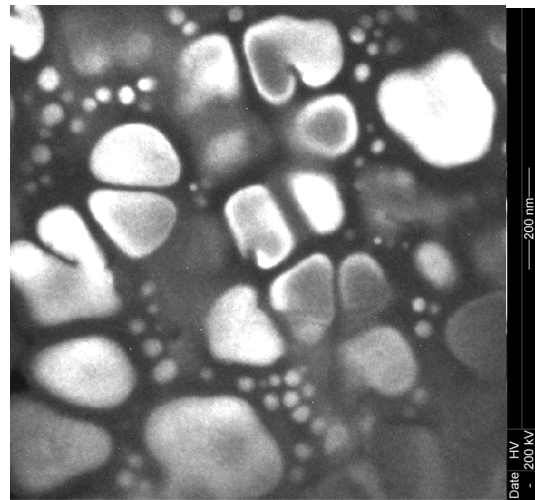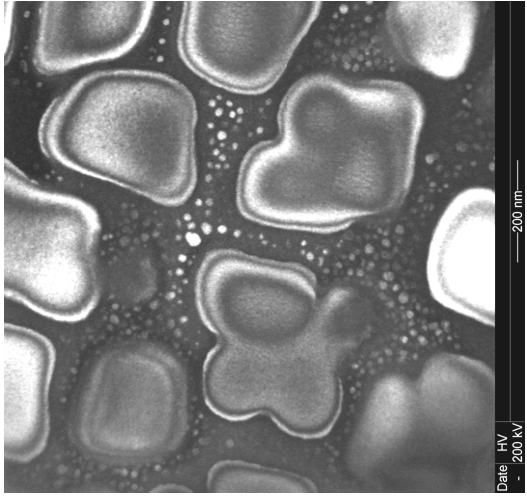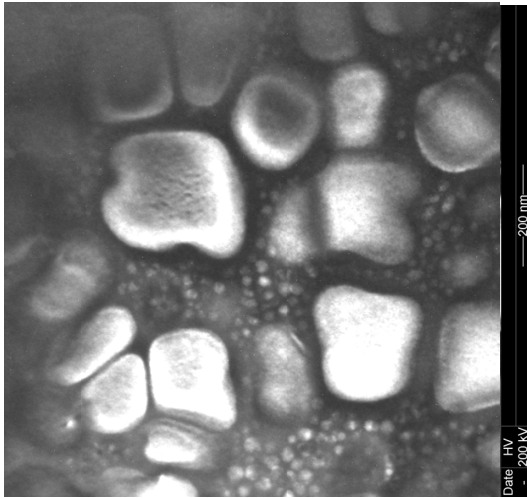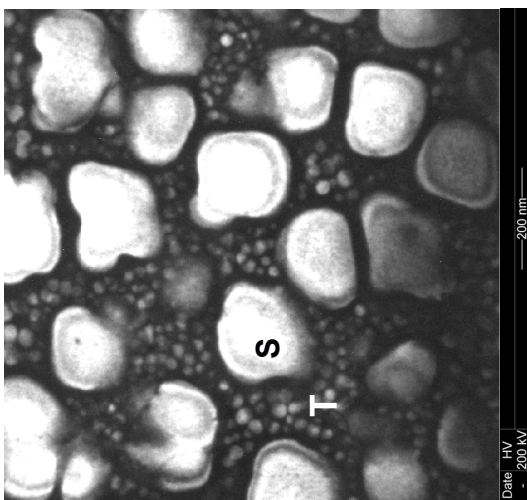
Figure 4.—a) Comparison of secondary (**S**) and tertiary (**T**) γ' for the six conditions of subscale LSHR.
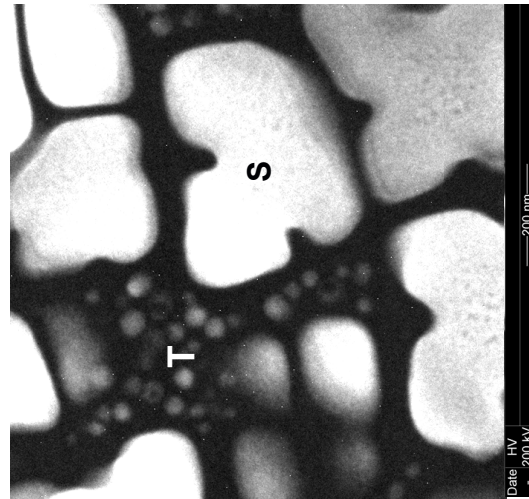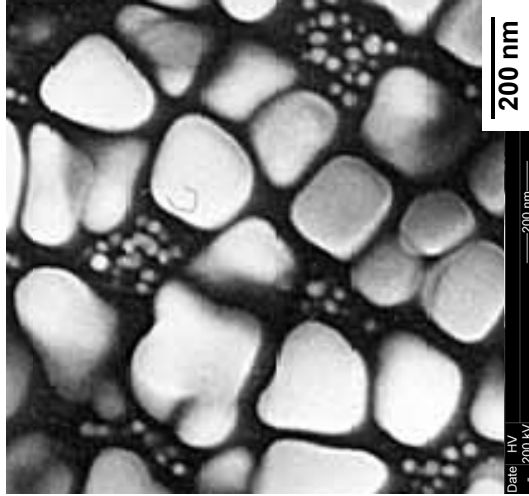
LSHR   ME3

Figure 4.—(Concluded) b) Comparison of secondary (**S**) and tertiary (**T**) γ' for production-scale LSHR and ME3.
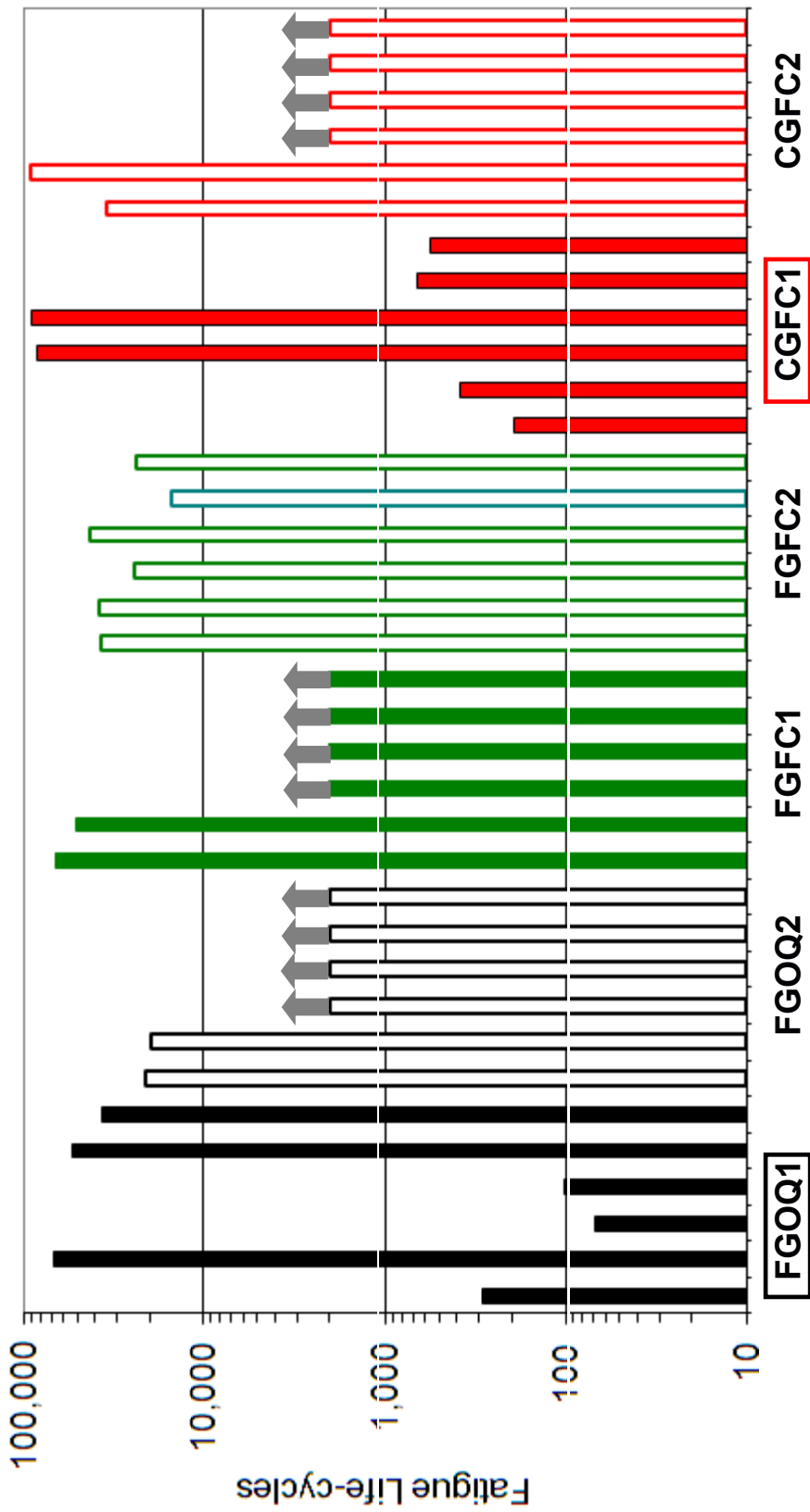
Figure 5.—Comparison of fatigue lives for the six conditions of subscale LSHR, tested in baseline 90 s maximum dwell fatigue cycle at a maximum net section stress of 790 MPa. Bimodal distribution of dwell fatigue lives are apparent for boxed conditions.
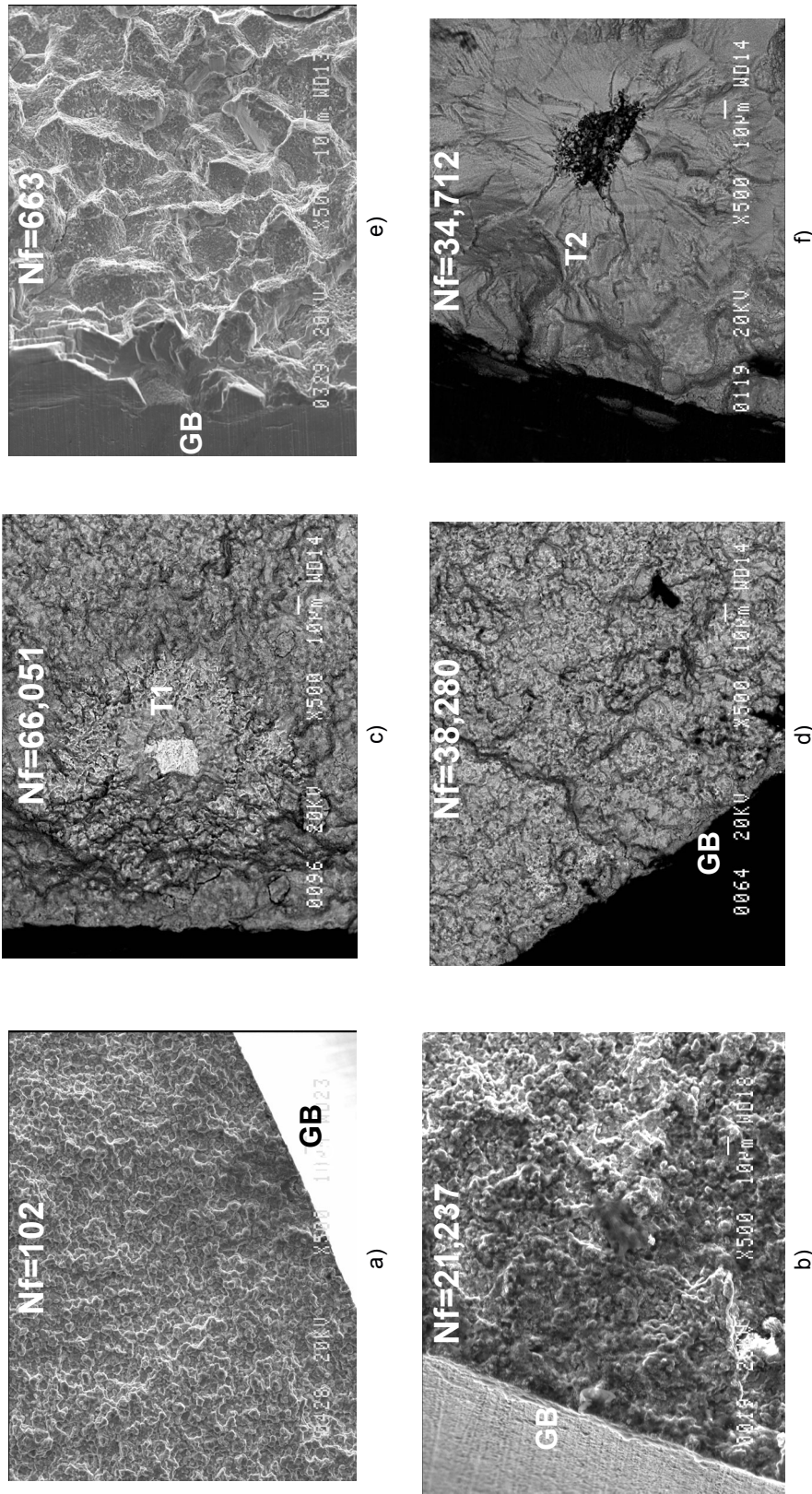
Figure 6.a.—Comparison of typical failure modes for the six LSHR conditions, tested in baseline maximum dwell fatigue cycle; a) FGOQ1; b) FGOQ2; c) FGFC1; d) FGFC2; e) CGFC1; and f) CGFC2. GB-Grain Boundary, T1-Type 1 Inclusion; and T2-Type 2 Inclusion.
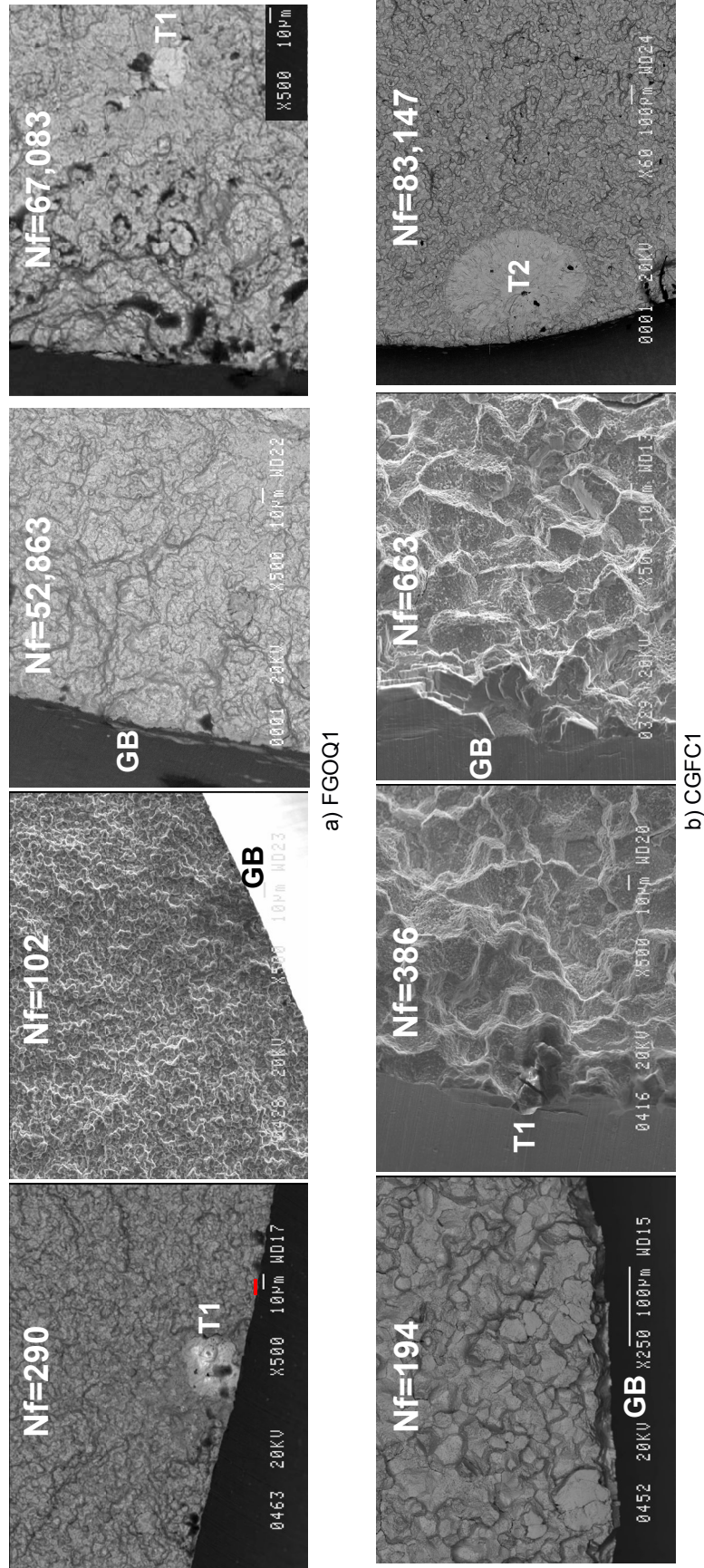
Figure 6.b.—Comparison of grain boundary and inclusion failure modes for a) FGOQ1 and b) CGFC1 conditions of subscale LSHR conditions, tested in baseline maximum dwell fatigue cycle. GB-Grain Boundary; T1-Type 1 Inclusion; and T2-Type 2 Inclusion.
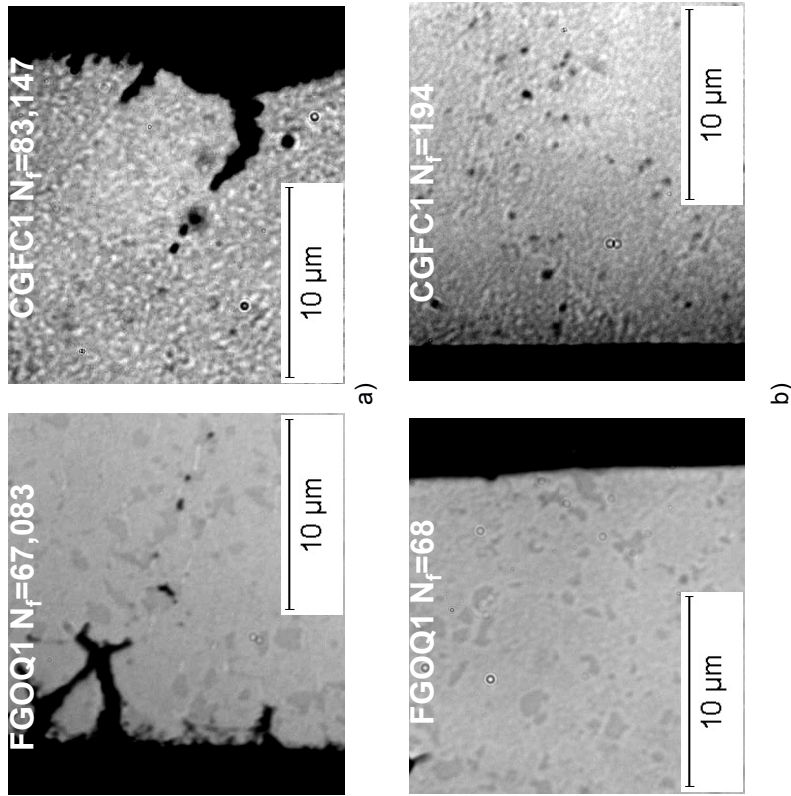
Figure 7.—Comparison of failure initiation sites and notch surface microstructures for a) long and b) short life specimens for FGOQ1 and CGFC1 subscale LSHR conditions, tested in baseline maximum dwell fatigue cycle.
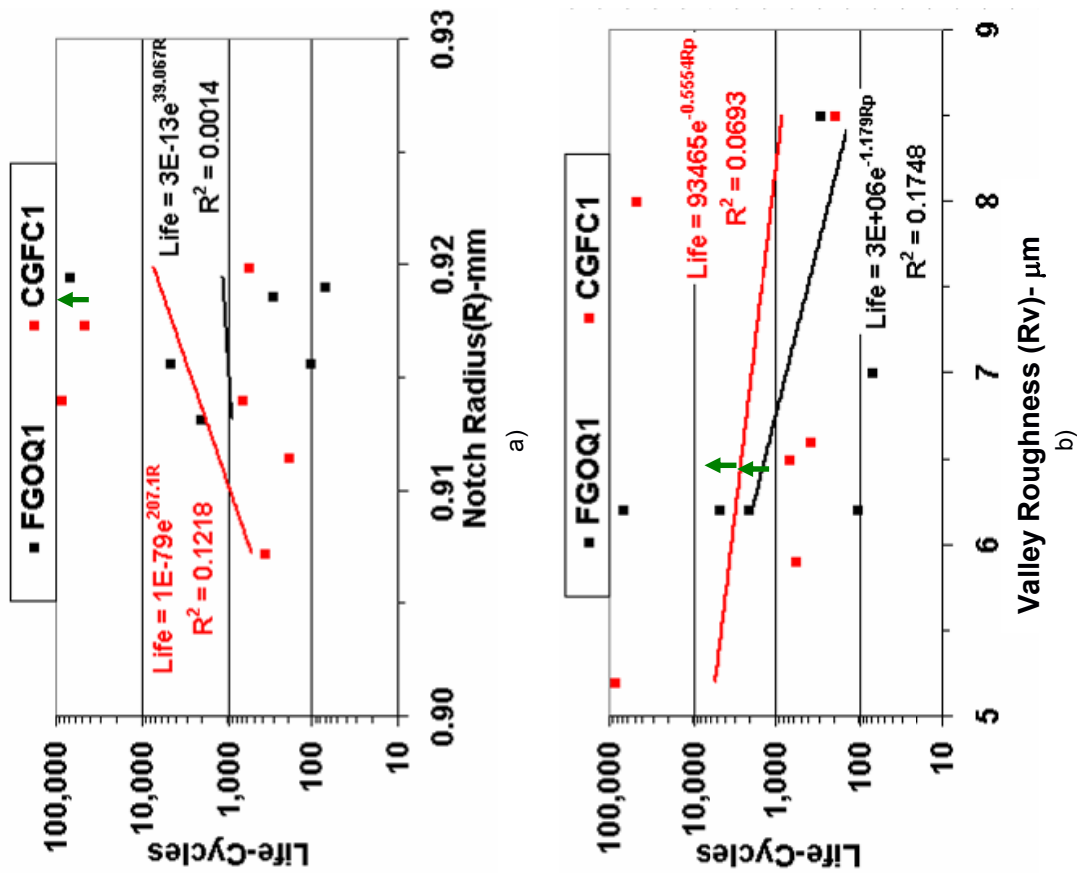
Figure 8.—Comparison of a) notch radius and b) roughness versus fatigue life, for FGOQ1 and CGFC1 conditions tested in baseline maximum dwell fatigue cycle.
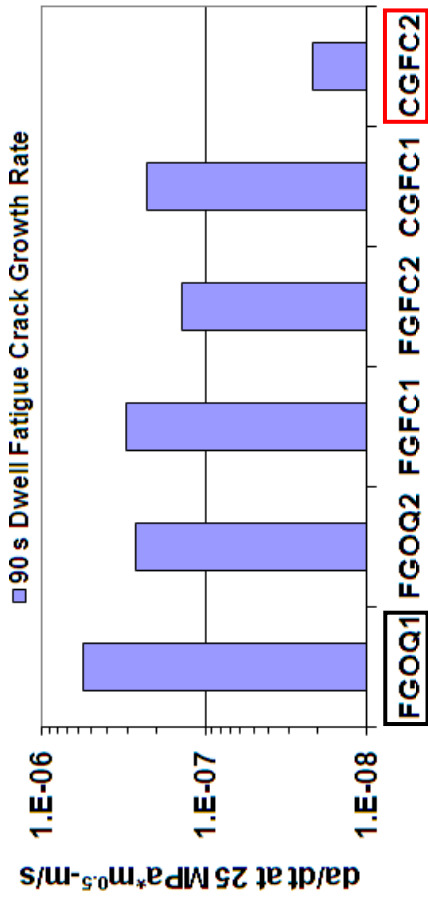
Figure 9.—Comparison of dwell crack growth rates measured for subscale LSHR conditions. Bimodal dwell fatigue lives were observed for boxed conditions.
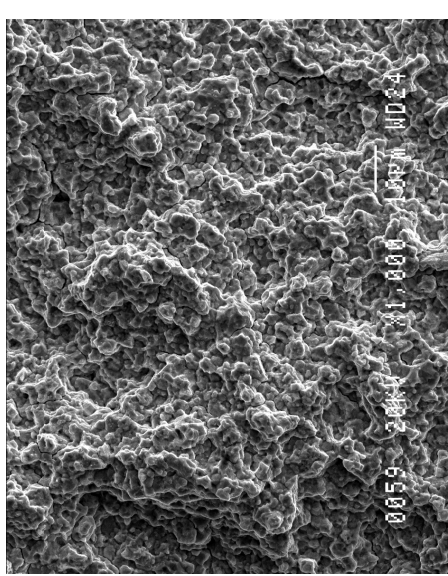
FGFC1
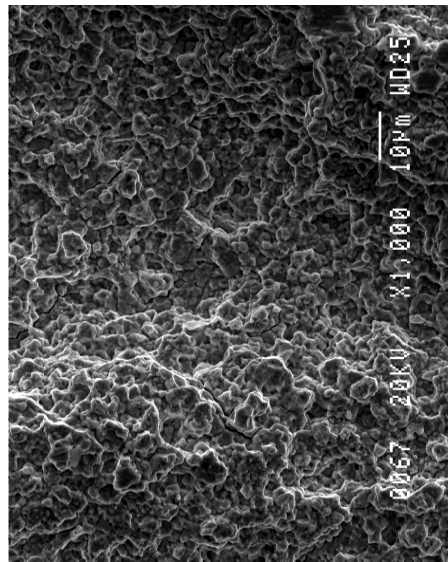
FGOQ2
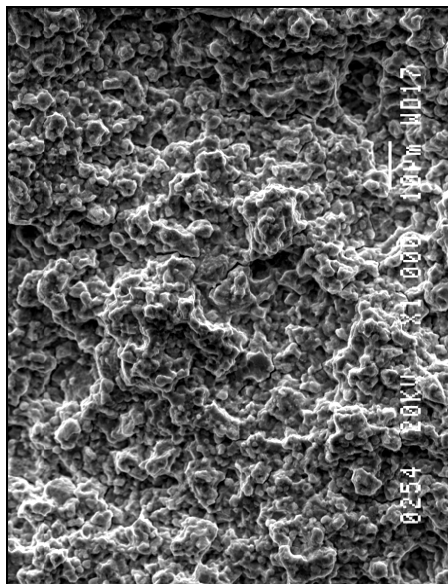
FGOQ1
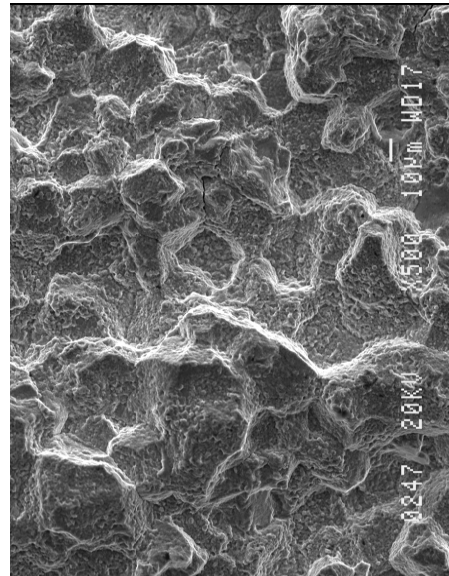
CGFC2
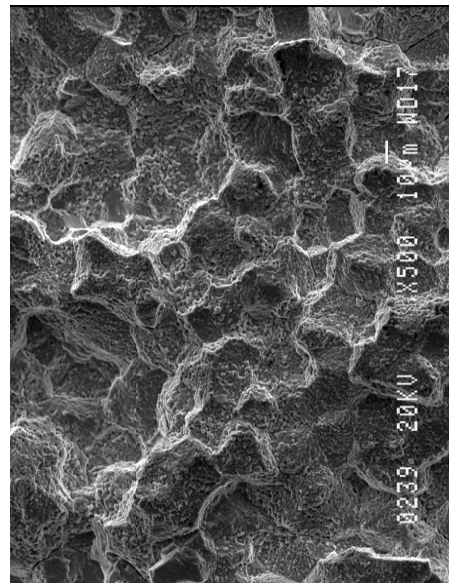
CGFC1
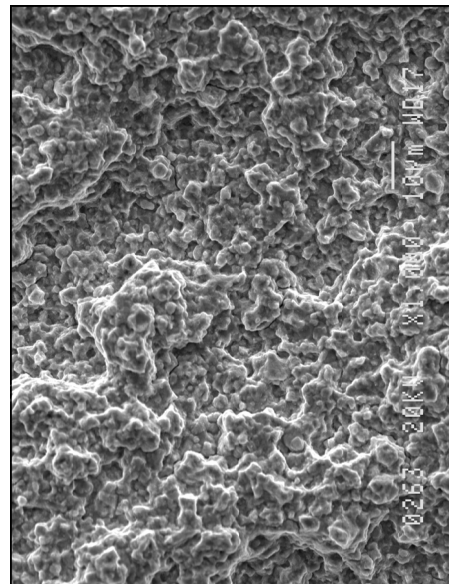
FGFC2

Figure 10.—Comparison of dwell crack growth modes for subscale LSHR conditions. Bimodal dwell fatigue lives were observed for boxed conditions.
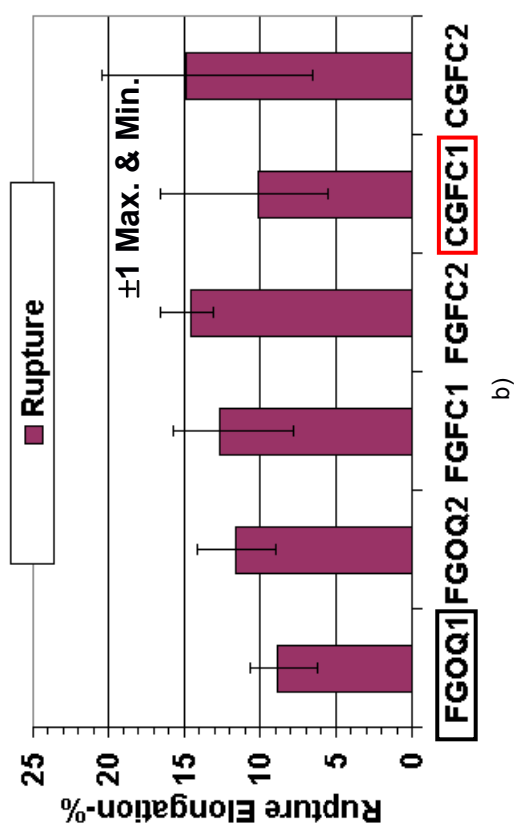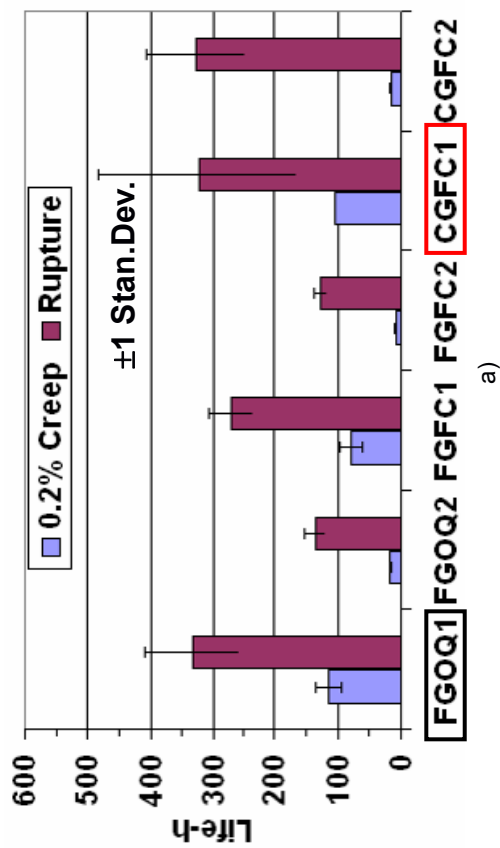
Figure 11.—Comparison of notch rupture properties for subscale LSHR conditions; a) life and b) smooth gage elongation. Bimodal dwell fatigue lives were observed for boxed conditions.
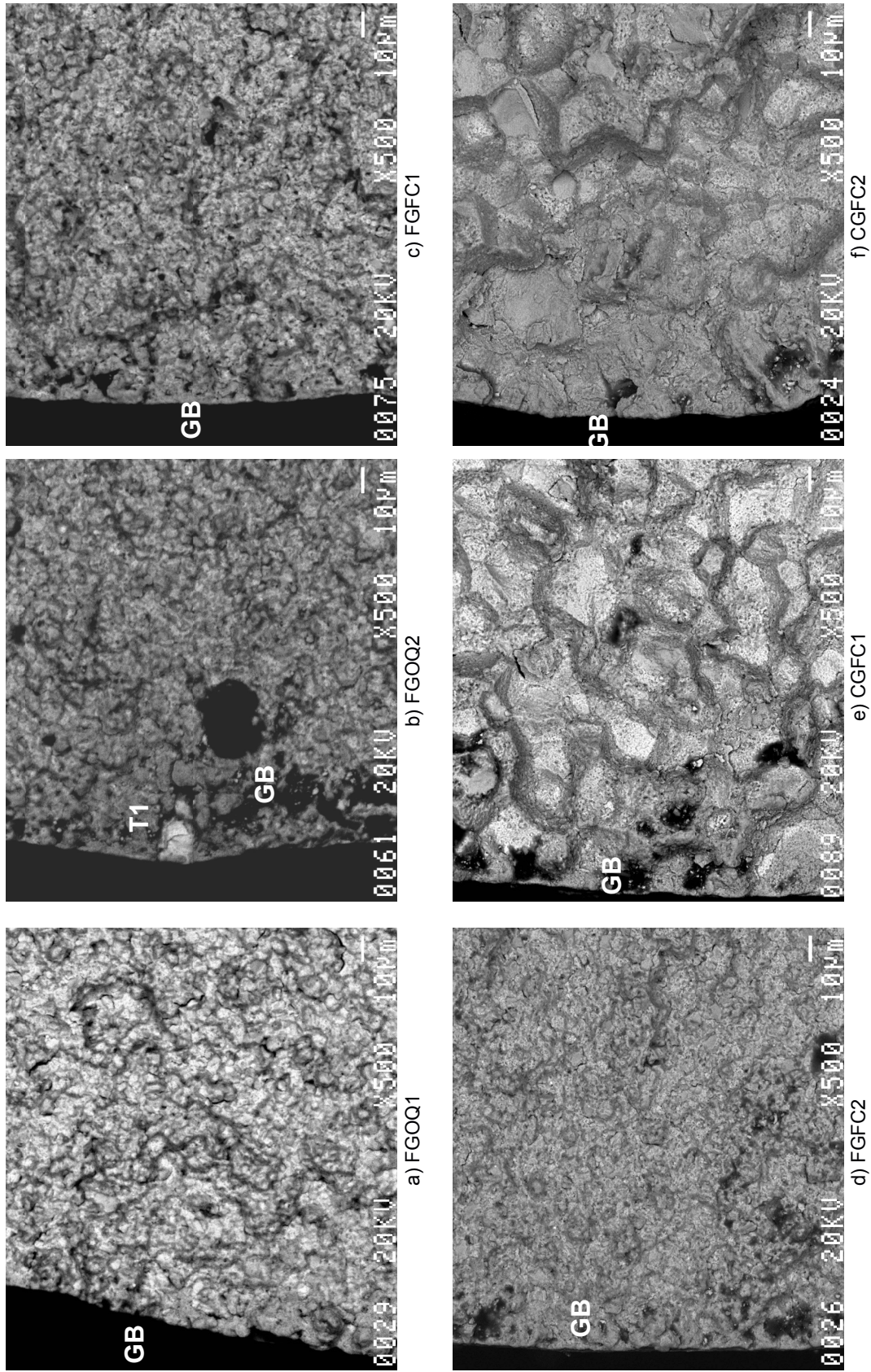
Figure 12.—Comparison of typical failure modes for rupture of subscale LSHR conditions.

a) FGOQ1

b) FGOQ2

c) FGFC1

d) FGFC2

e) CGFC1

f) CGFC2
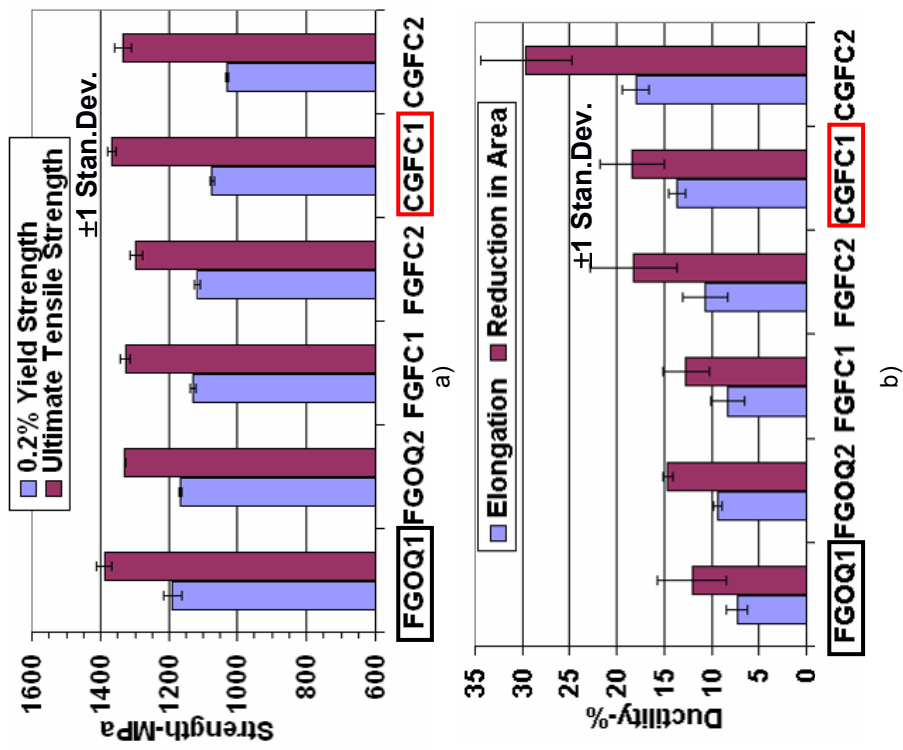
Figure 13.—Comparison of tensile properties for subscale LSHR conditions; a) strength and b) ductility. Bimodal dwell fatigue lives were observed for boxed conditions.
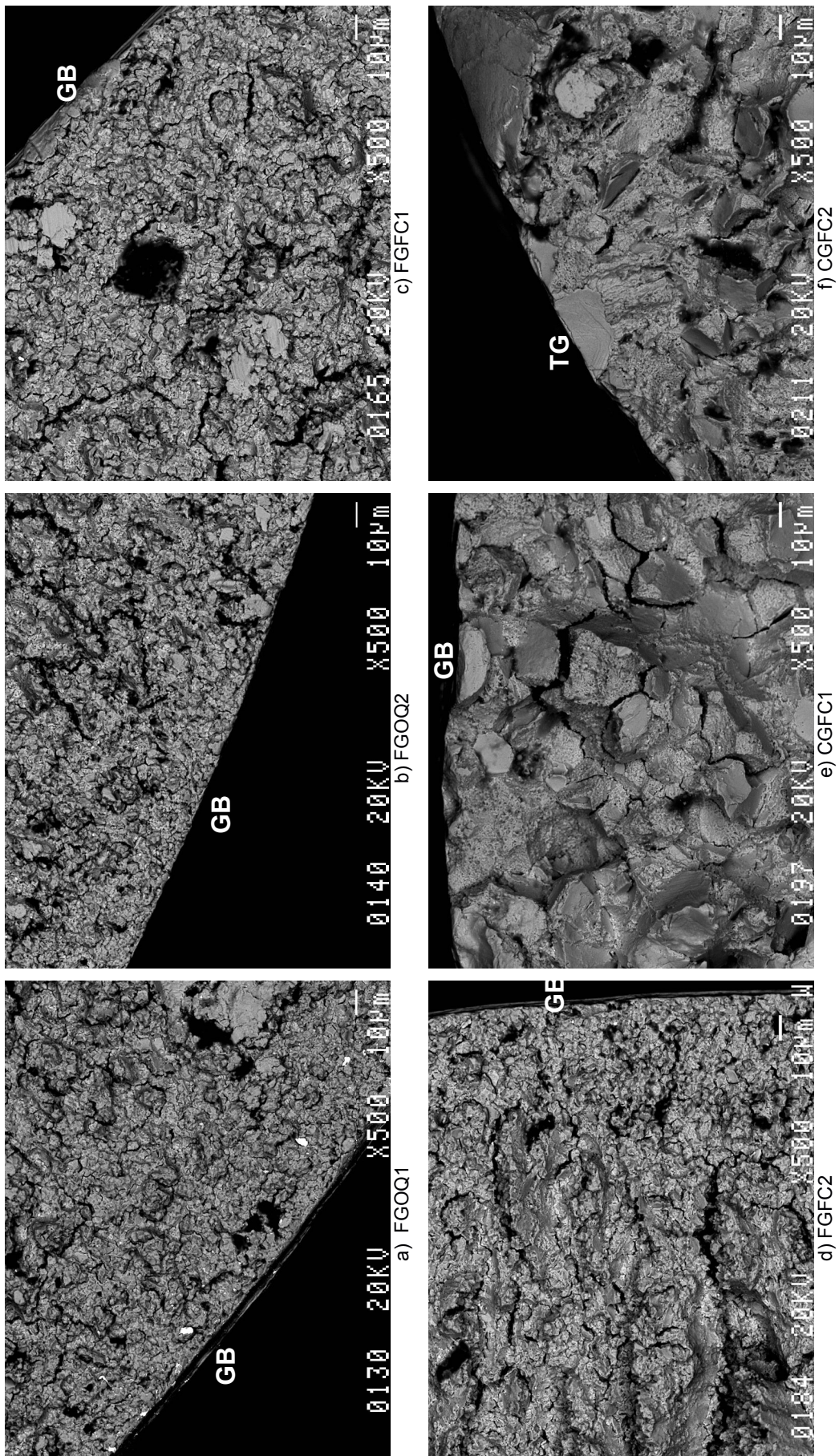
Figure 14.—Comparison of typical failure modes for tensile tests of subscale LSHR conditions; TG-Transgranular.
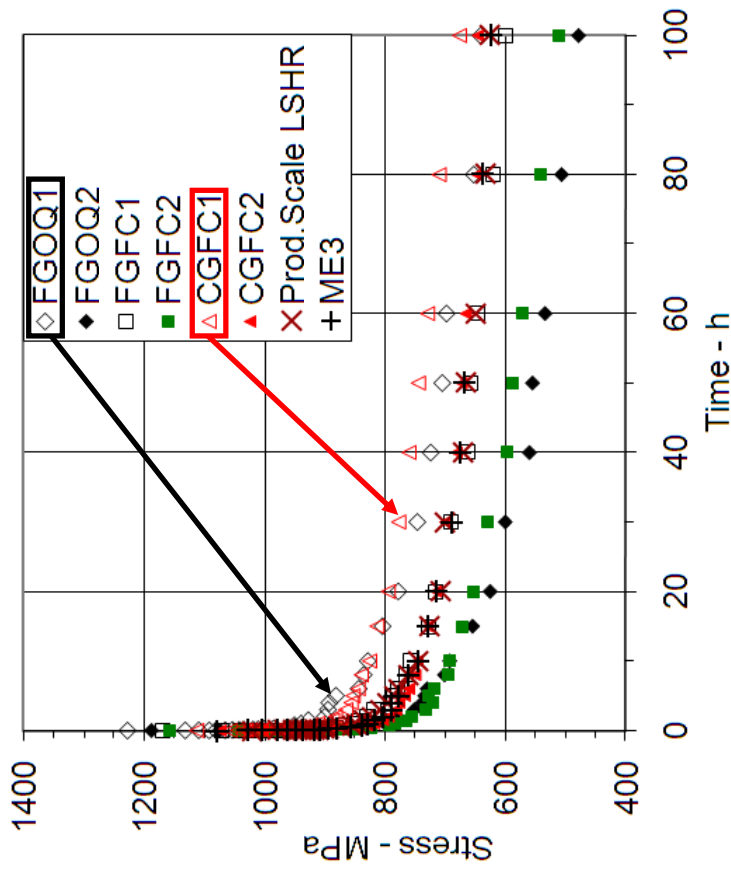
Figure 15.—Comparison of stress relaxation versus time for all tested materials. Bimodal dwell fatigue lives were observed for boxed conditions.
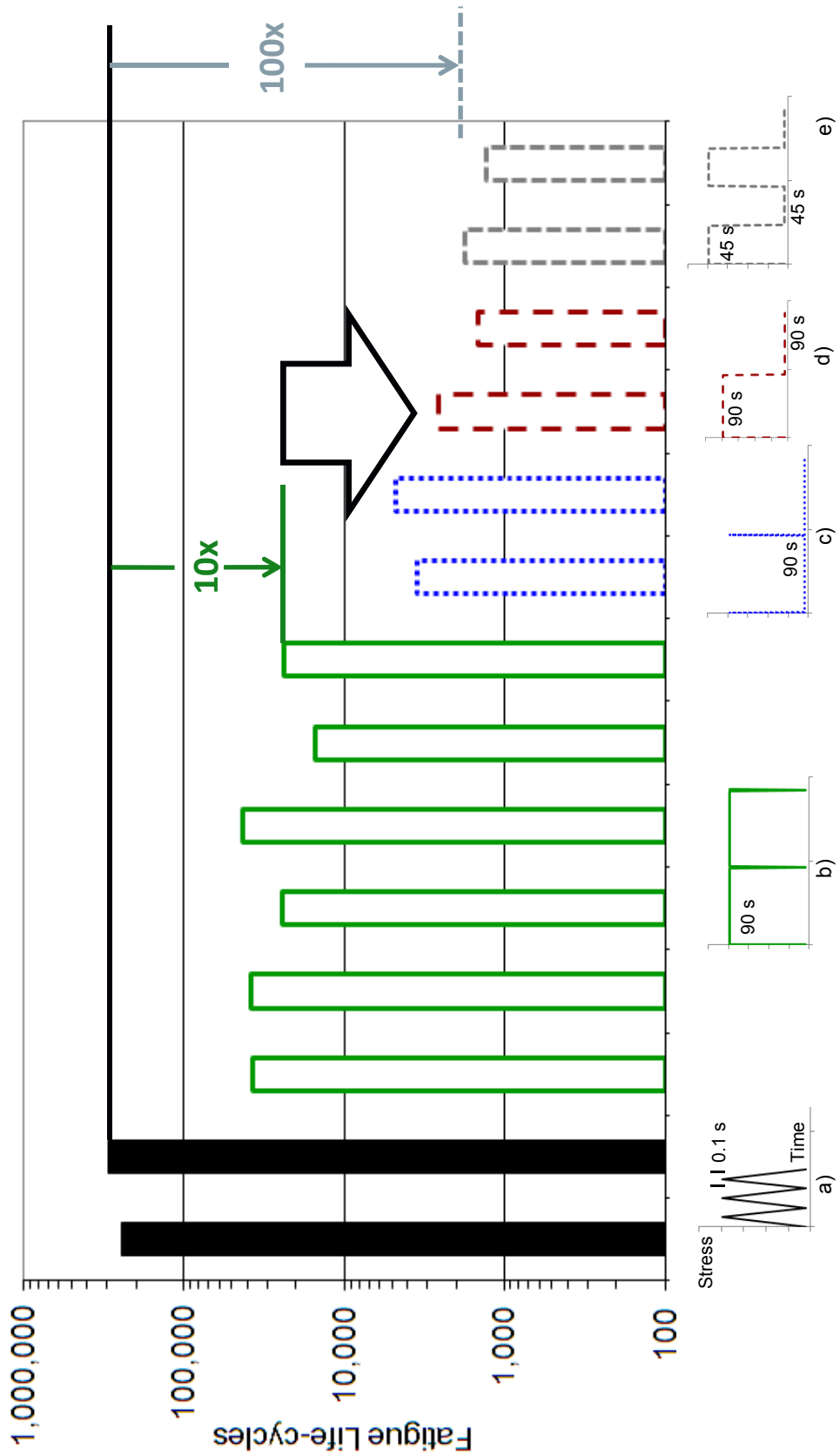
Figure 16.—Effects of cycle profile on fatigue life for subscale LSHR FGFC2 condition; a) no-dwell; b) 90 s maximum dwell; c) 90 s maximum-minimum dwell; d) 90 s maximum-minimum dwell; and e) 45 s maximum-minimum dwell.
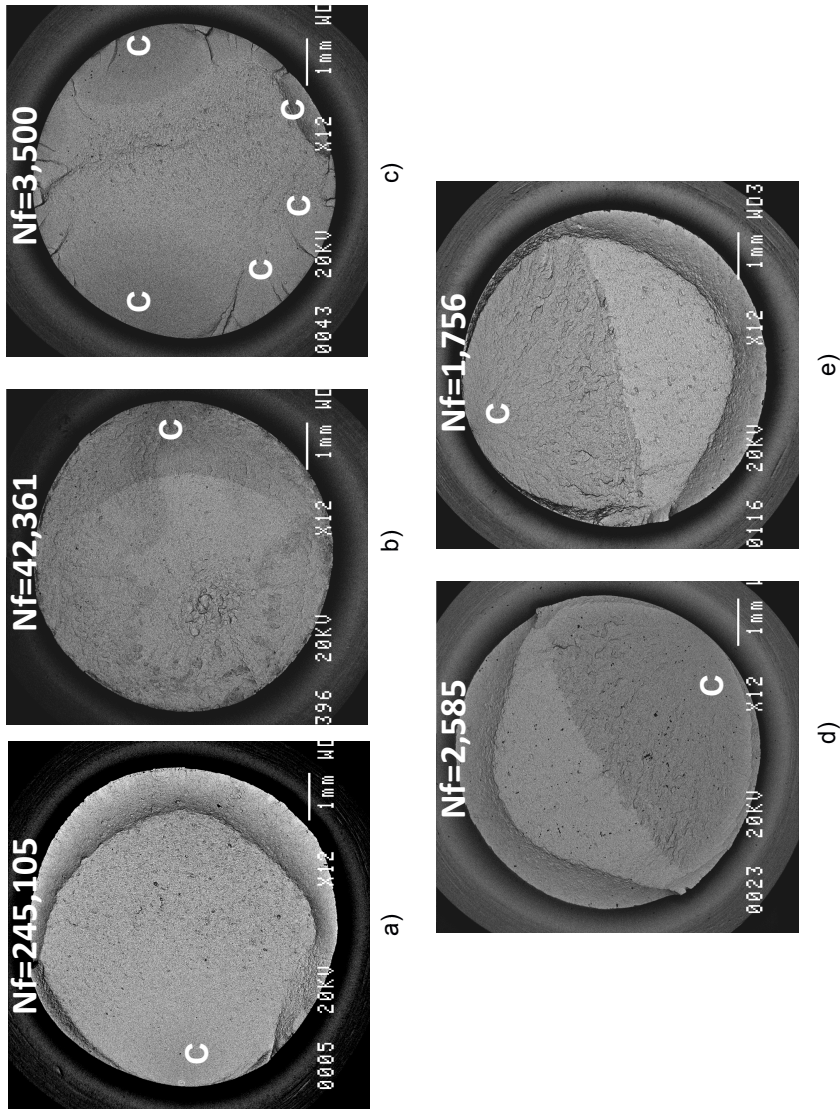
Figure 17.—Effects of cycle profile on crack frequency for subscale LSHR FGFC2 condition; a) no-dwell; b) 90 s maximum dwell; c) 90 s minimum dwell; d) 90 s maximum-minimum dwell; and e) 45 s maximum-minimum dwell. C-Crack initiation.
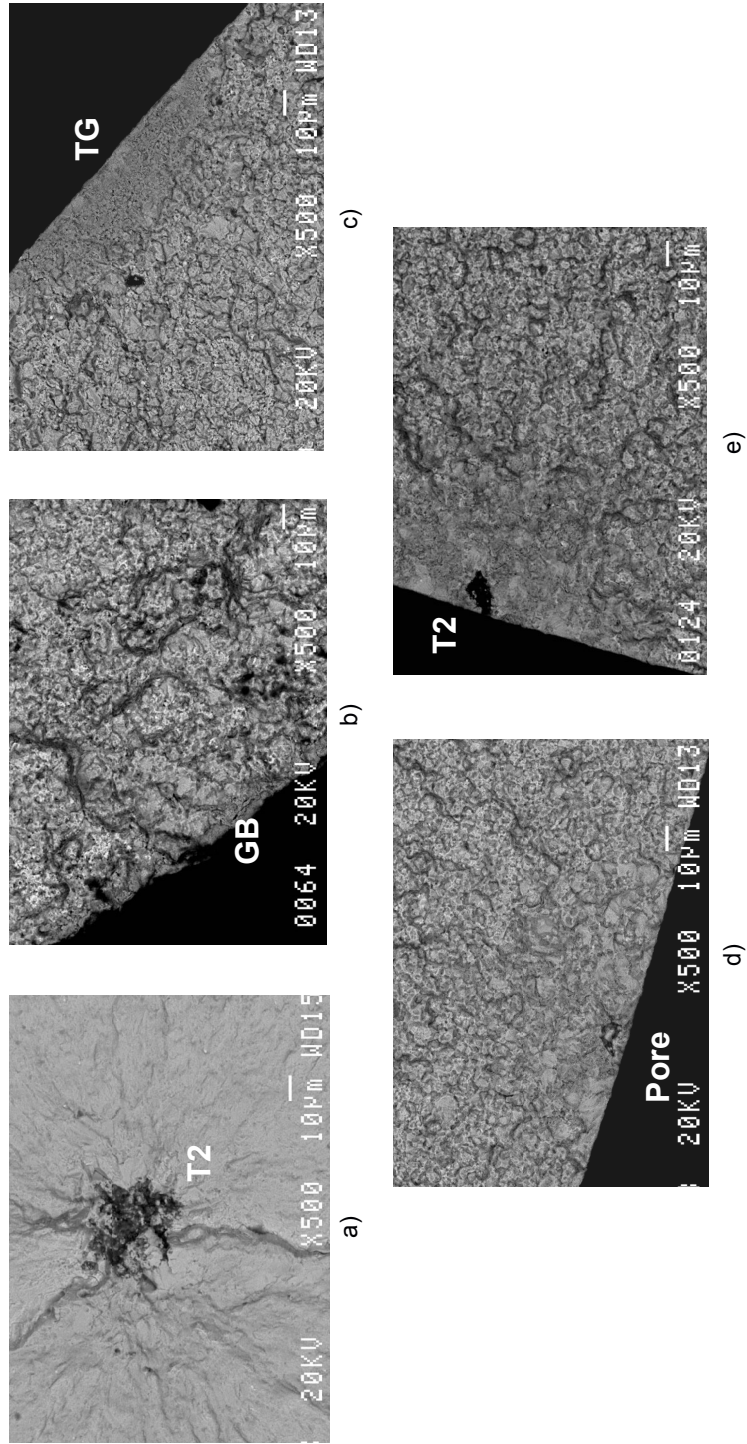
Figure 18.—Effects of cycle profile on typical crack initiation modes for LSHR FGFC2 condition; a) no-dwell; b) 90 s maximum dwell; c) 90 s minimum dwell; d) 90 s maximum-minimum dwell; and e) 45 s maximum-minimum dwell. GB-Grain Boundary, TG-Transgranular; T1-T1 Inclusion; and T2-T2 Inclusion.
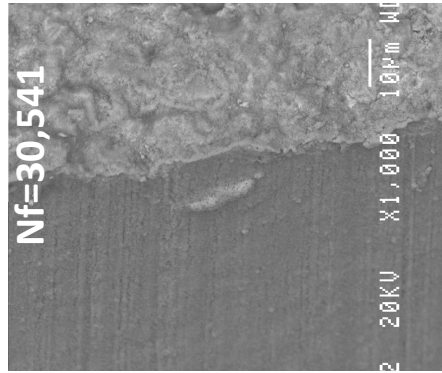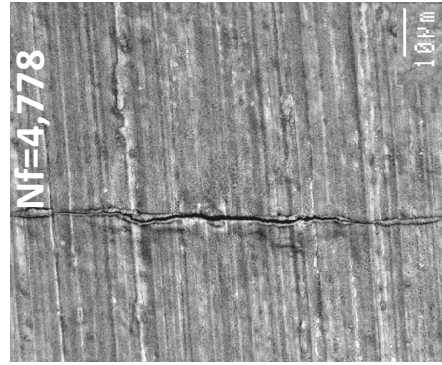
Figure 19.—Comparison of secondary cracks on the notch surface, adjacent to the primary failure initiation point for LSHR FGFC2 condition; a) 90 s maximum dwell and b) 90 s minimum dwell. Loading direction is horizontal.
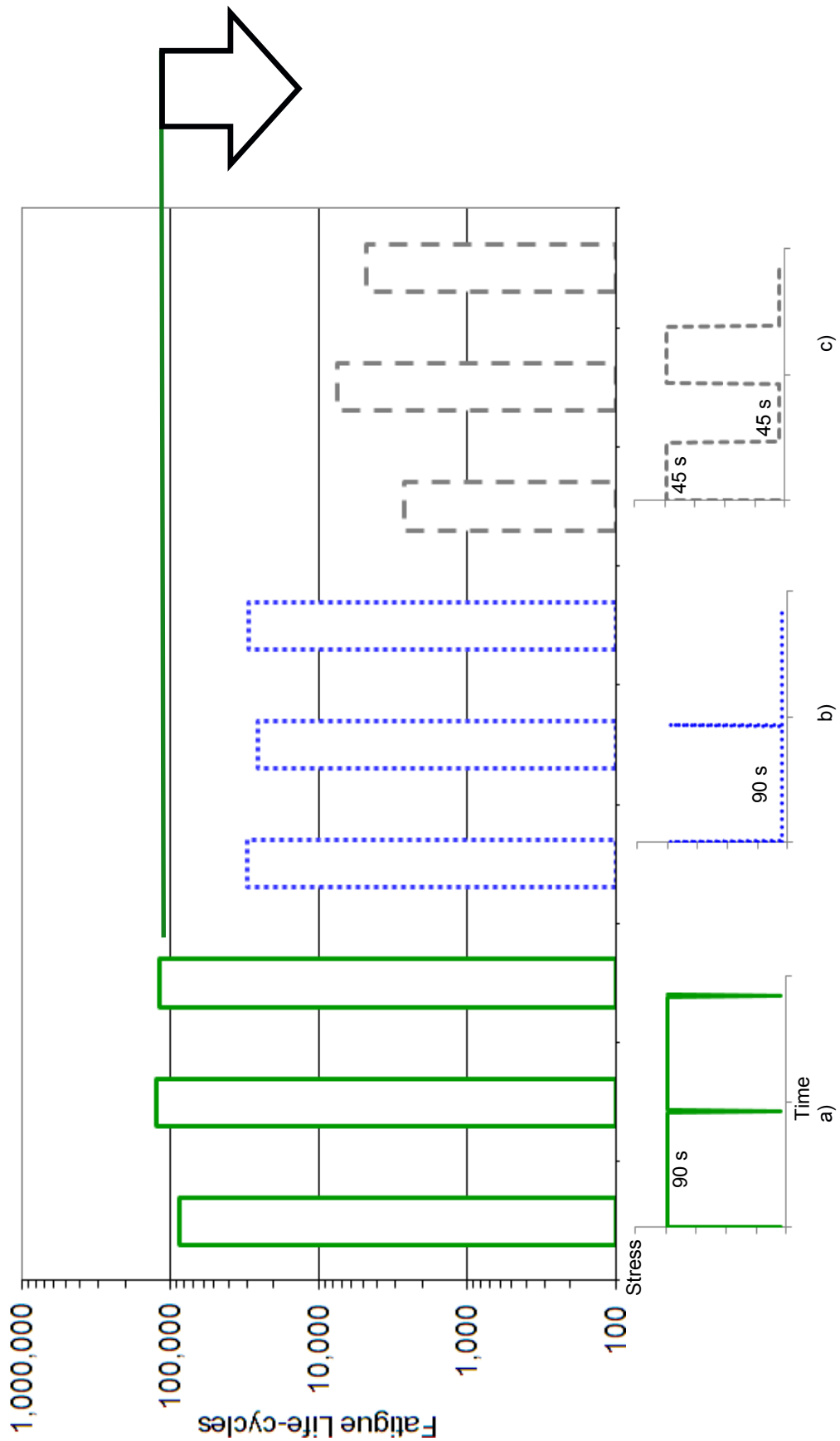
Figure 20.—Effects of cycle profile on fatigue life for production-scale coarse-grain LSHR; a) maximum dwell; b) minimum dwell; and c) 45 s maximum-minimum dwell.
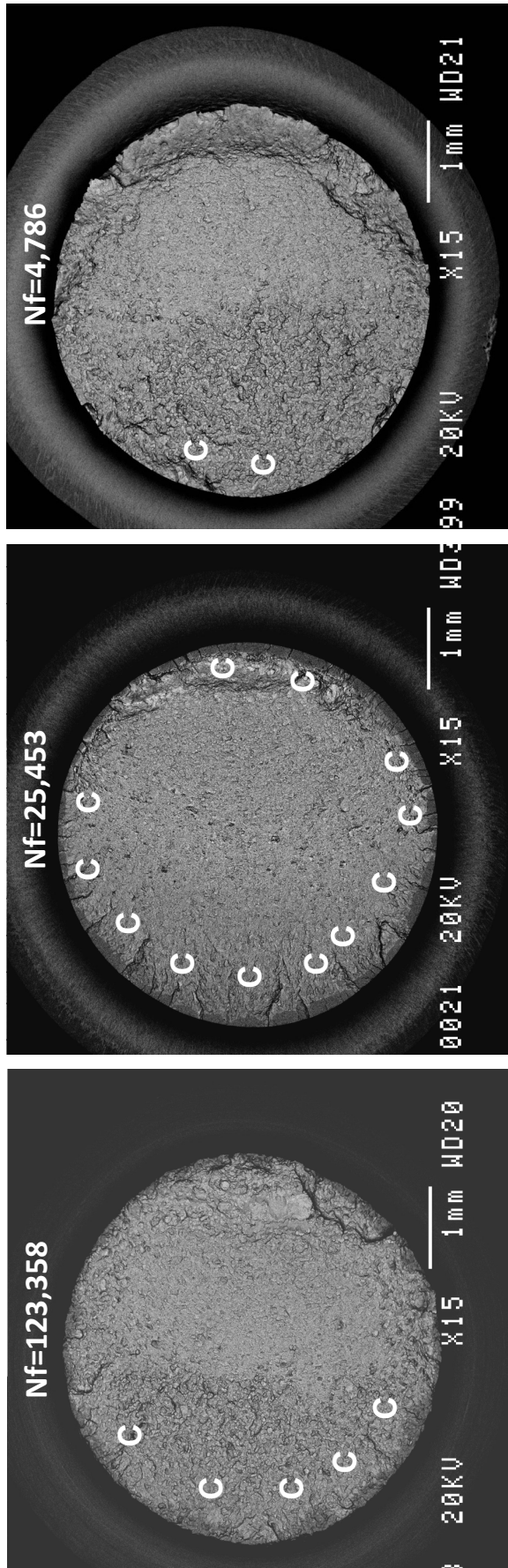
Figure 21.—Effects of cycle profile on crack frequency for coarse-grain LSHR; a) 90 s maximum dwell; b) 90 s minimum dwell; and c) 45 s maximum-minimum dwell. C-Crack initiation.
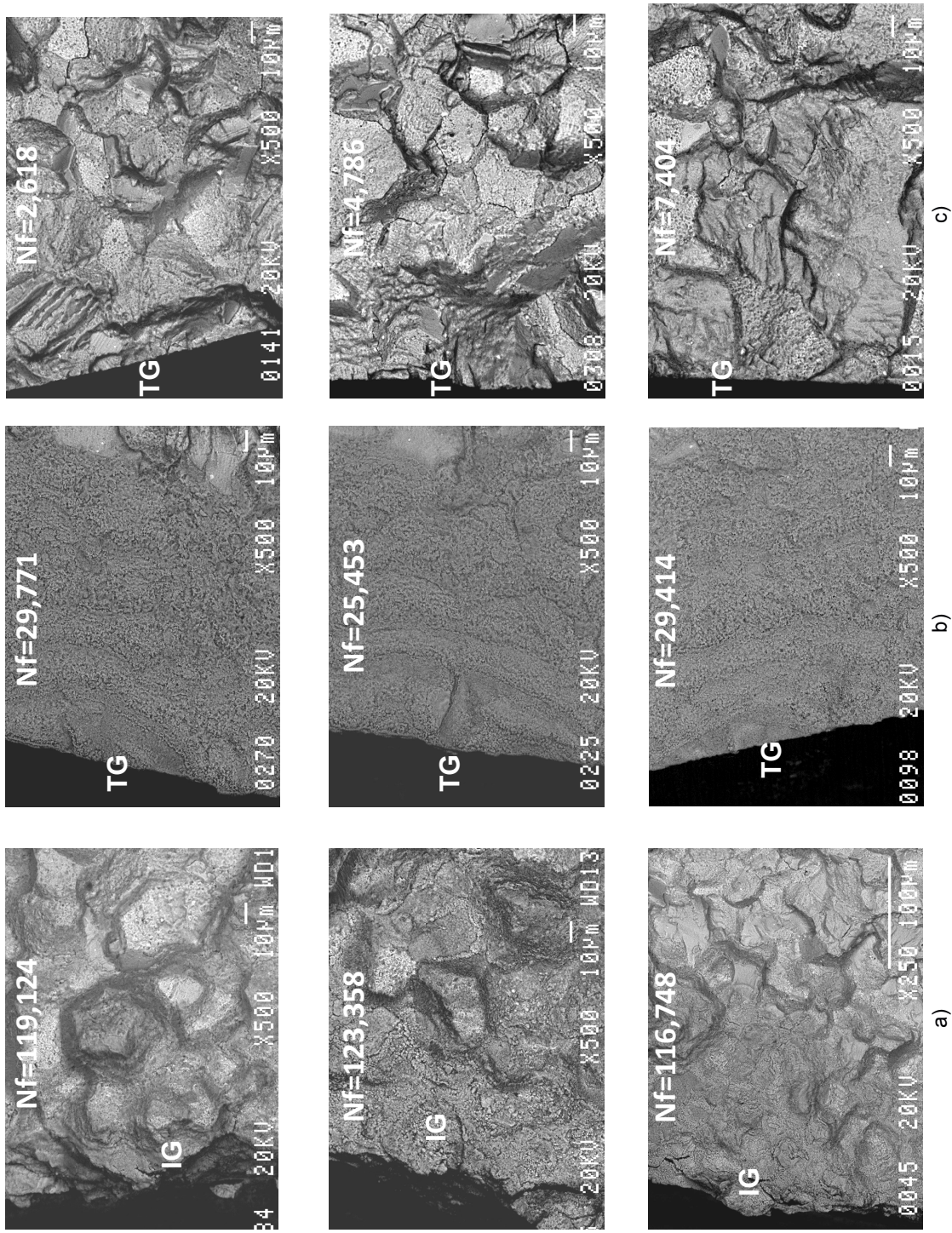
Figure 22.—Effects of cycle profile on crack initiation modes for all test specimens of production-scale coarse-grain LSHR; a) 90 s maximum dwell; b) 90 s minimum dwell; and c) 45 s maximum-minimum dwell. IG-Intergranular and TG-Transgranular.
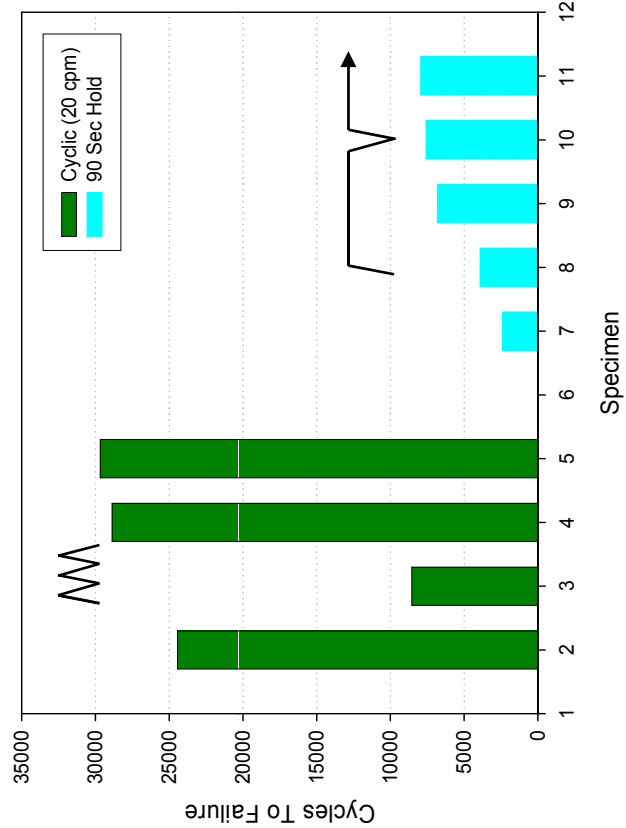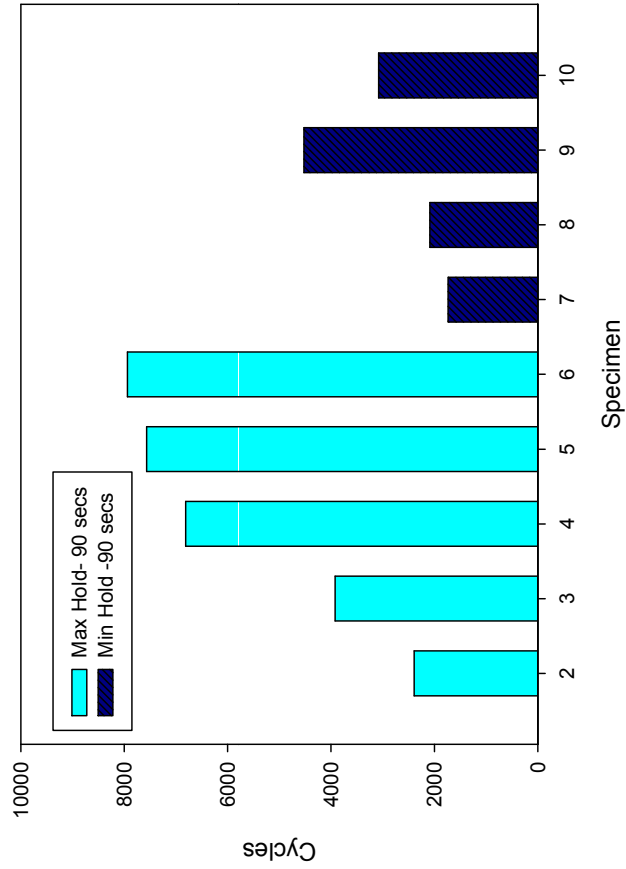
Figure 23.—Effects of cycle profile on fatigue life for production-scale coarse-grain ME3.
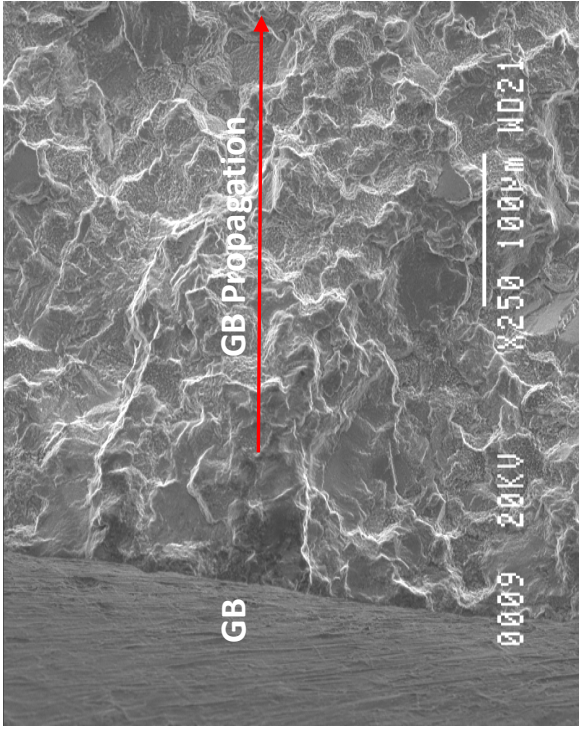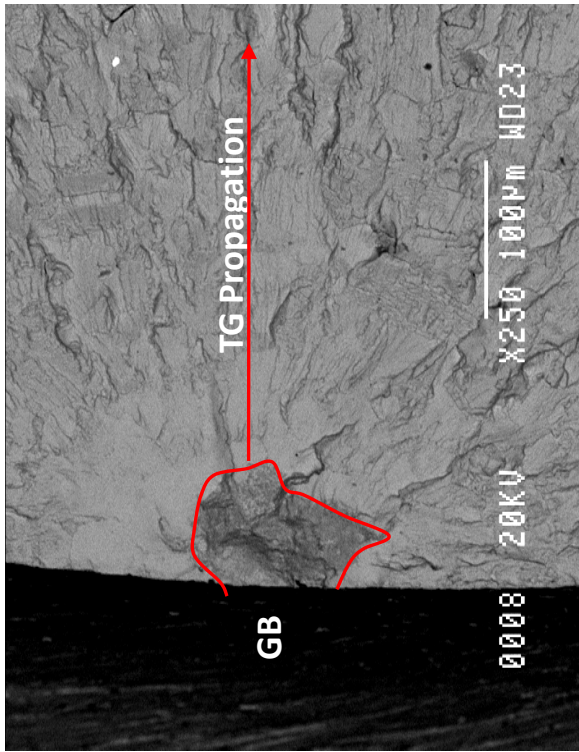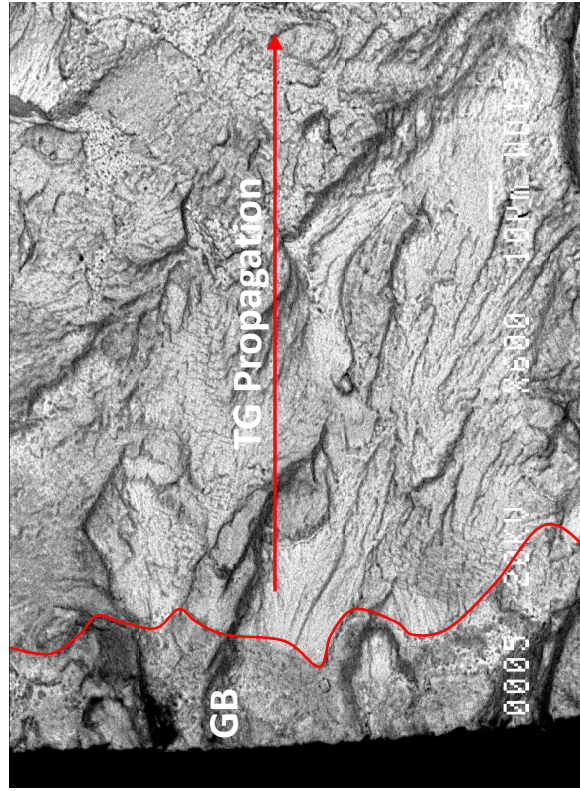
Figure 24.—Comparison of failure initiation modes versus cycle profile for coarse-grain ME3; a) no-dwell; b) 90 s maximum dwell; and c) 90 s minimum dwell. GB-Grain Boundary.
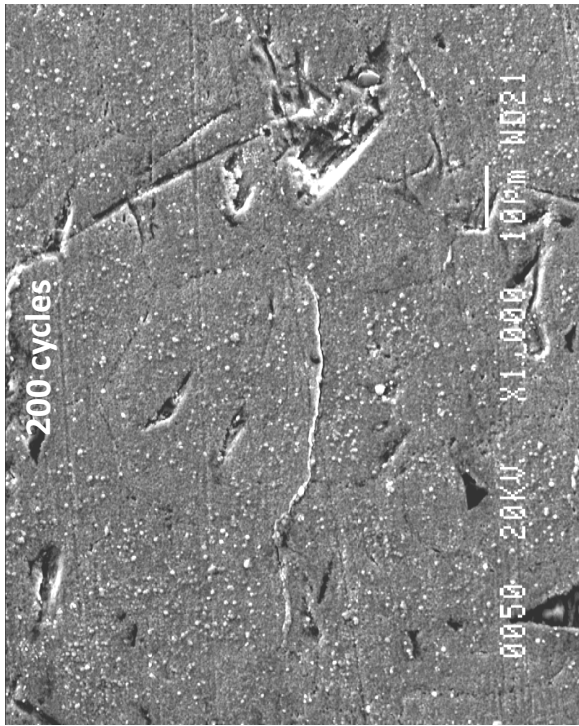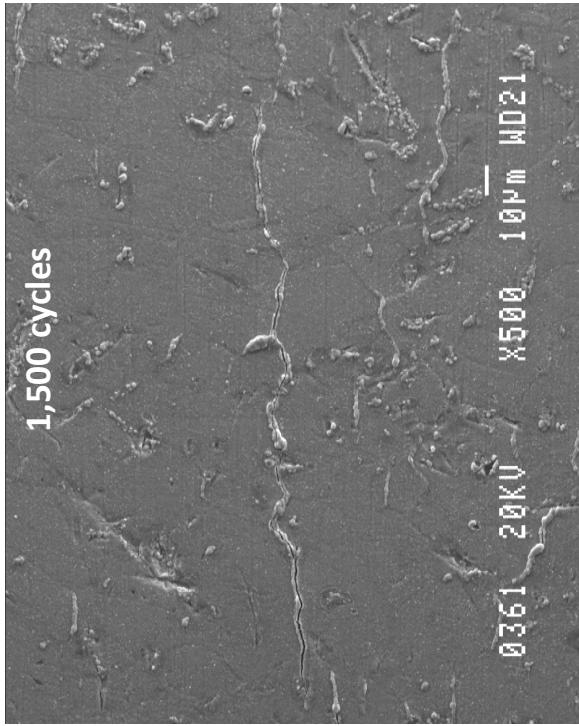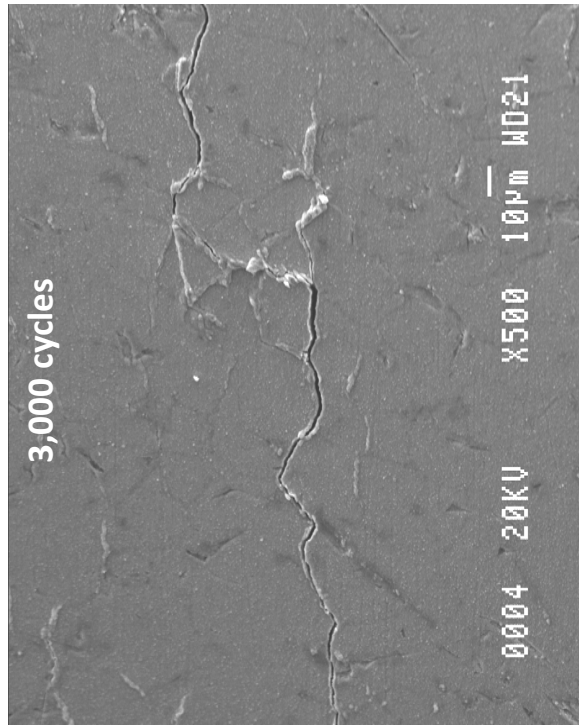
Figure 25.—Notch surface cracks for interrupted 90 s minimum dwell test of coarse-grain ME3, which failed at 3,080 cycles; a) 200 cycles; b) 1,500 cycles; and c) 3,000 cycles. Loading direction is vertical.
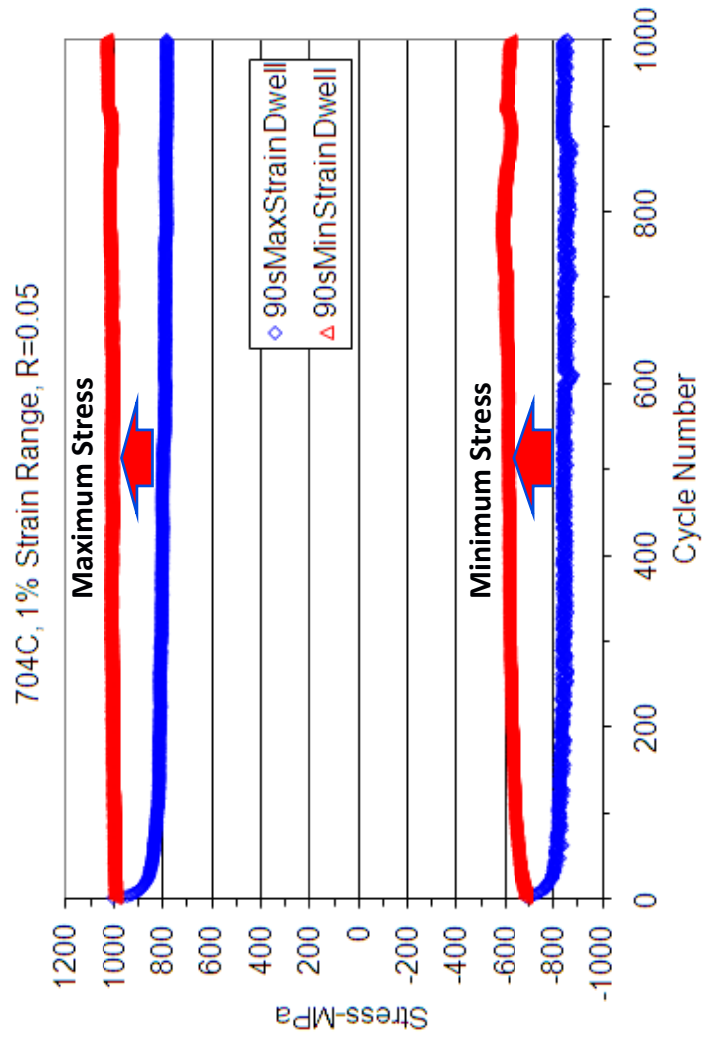
Figure 26.—Comparison of maximum and minimum stress versus cycles for strain-controlled tests of coarse-grain ME3 with dwells at maximum or minimum strain.
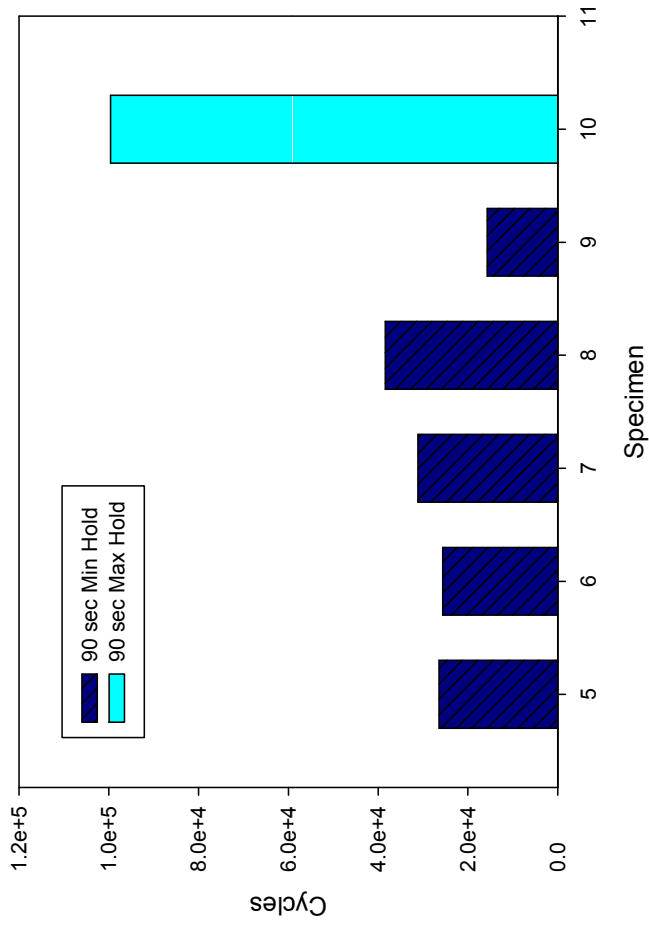
Figure 27.—Comparison of cyclic lives for strain-controlled tests of coarse-grain ME3 with 90 s dwells at maximum or minimum strain.
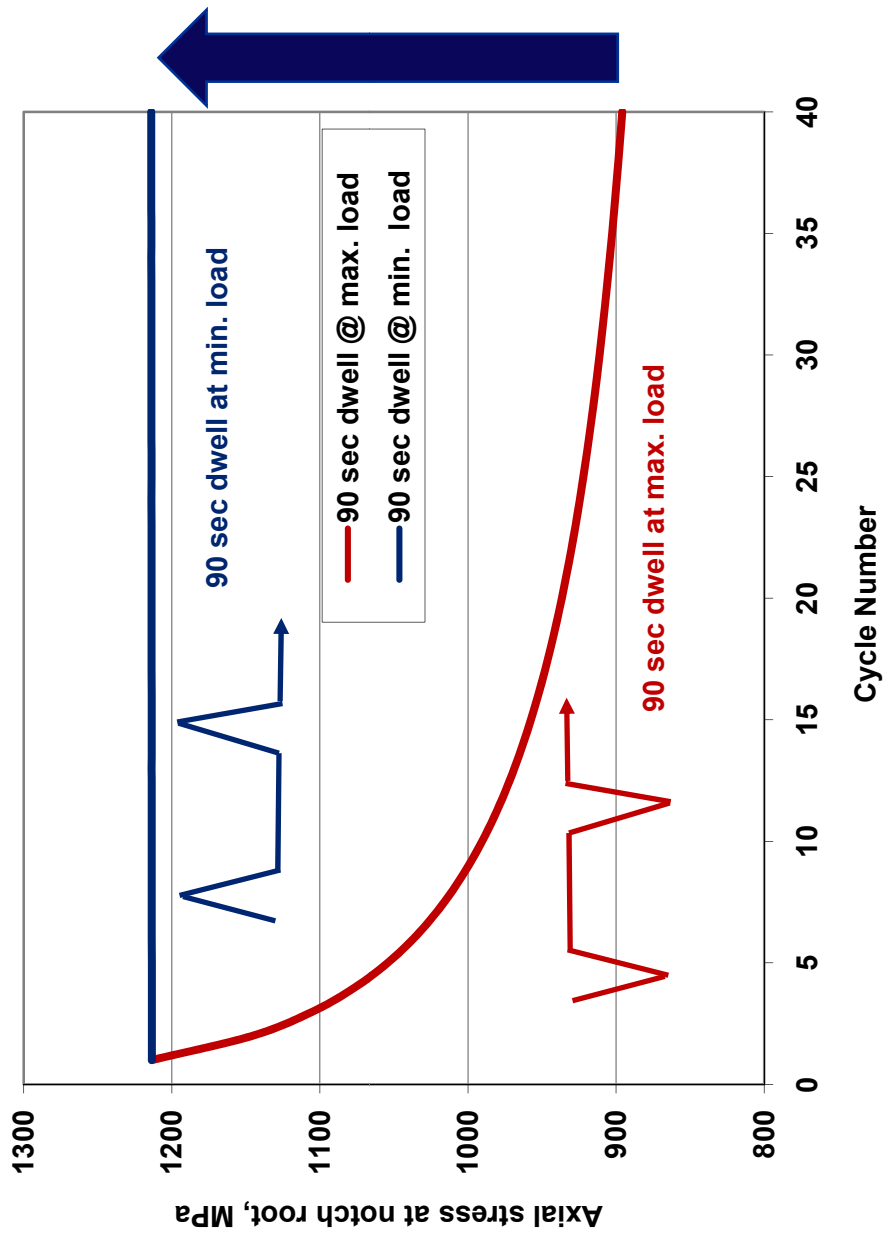
Figure 28.—Maximum axial stress at the notch root versus cycles predicted by visco-plastic finite element analysis for notch fatigue tests of coarse-grain ME3 with dwells at maximum or minimum stress.

Test Type	Notch Root Max Stress	Notch Root Min Stress
Cyclic (0.33 Hz)	1213.5 MPa	-475.8 MPa
90 s Min Dwell	1214.2 MPa	-475.1 MPa
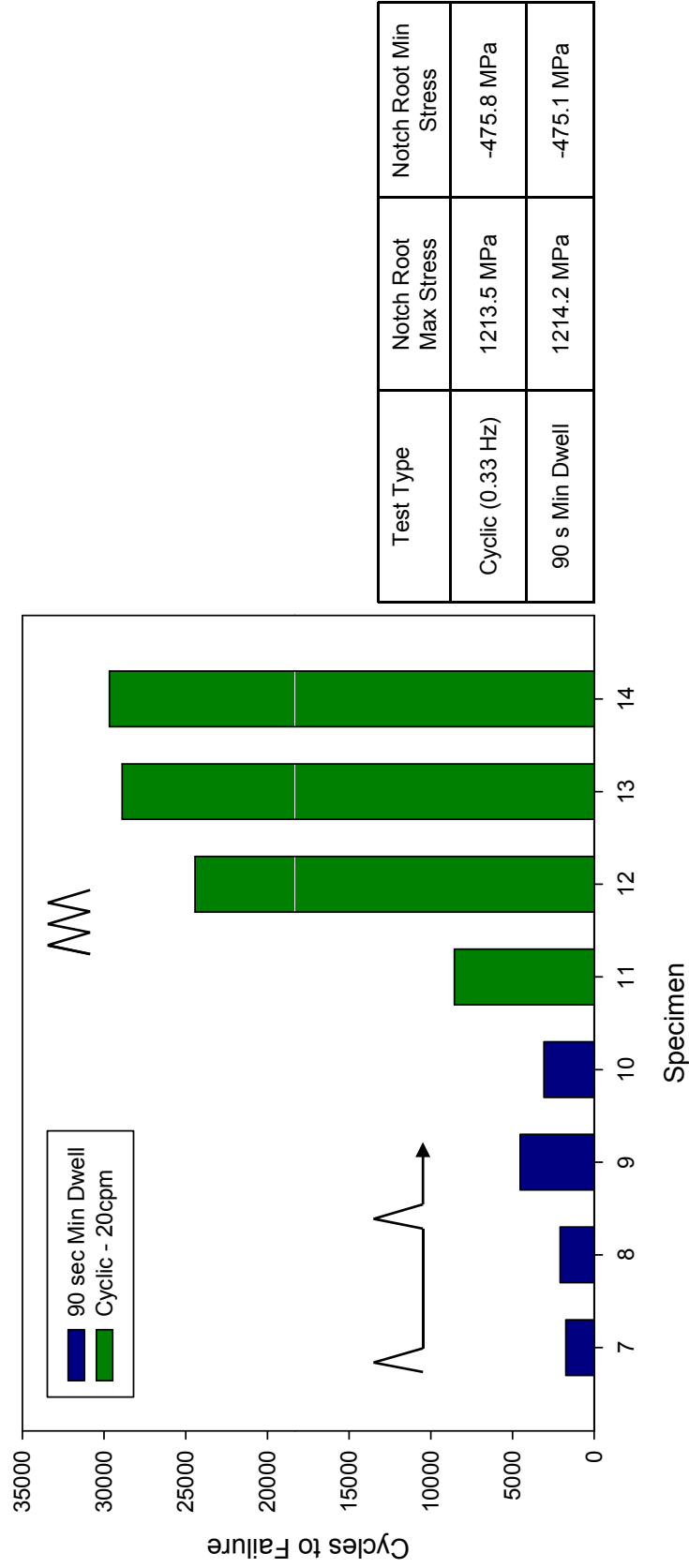
Figure 29.—Comparison of notch fatigue lives for cyclic no-dwell and 90 s minimum dwell tests of coarse-grain ME3, having comparable predicted maximum and minimum axial stresses at the notch root.

REPORT DOCUMENTATION PAGE

1. REPORT DATE (DD-MM-YYYY) 01-06-2011	2. REPORT TYPE Technical Memorandum	3. DATES COVERED (From - To)

4. TITLE AND SUBTITLE
Factors Influencing Dwell Fatigue Cracking in Notches of Powder Metallurgy Superalloys

5a. CONTRACT NUMBER

5b. GRANT NUMBER

5c. PROGRAM ELEMENT NUMBER

6. AUTHOR(S)
Gabb, T., P.; Telesman, J.; Ghosn, L.; Garg, A.; Gayda, J.

5d. PROJECT NUMBER

5e. TASK NUMBER

5f. WORK UNIT NUMBER
WBS 284848.02.02.03.01.01

7. PERFORMING ORGANIZATION NAME(S) AND ADDRESS(ES)
National Aeronautics and Space Administration
John H. Glenn Research Center at Lewis Field
Cleveland, Ohio 44135-3191

8. PERFORMING ORGANIZATION REPORT NUMBER
E-17805

9. SPONSORING/MONITORING AGENCY NAME(S) AND ADDRESS(ES)
National Aeronautics and Space Administration
Washington, DC 20546-0001

10. SPONSORING/MONITOR'S ACRONYM(S)
NASA

11. SPONSORING/MONITORING REPORT NUMBER
NASA/TM-2011-217118

12. DISTRIBUTION/AVAILABILITY STATEMENT
Unclassified-Unlimited
Subject Category: 07
Available electronically at http://www.sti.nasa.gov
This publication is available from the NASA Center for AeroSpace Information, 443-757-5802

13. SUPPLEMENTARY NOTES

14. ABSTRACT
The influences of heat treatment and cyclic dwells on the notch fatigue resistance of powder metallurgy disk superalloys were investigated for low solvus high refractory (LSHR) and ME3 disk alloys. Disks were processed to produce material conditions with varied microstructures and associated mechanical properties. Notched specimens were first subjected to baseline dwell fatigue cycles having a dwell at maximum load, as well as tensile, stress relaxation, creep rupture, and dwell fatigue crack growth tests at 704 °C. Several material heat treatments displayed a bimodal distribution of fatigue life with the lives varying by two orders-of-magnitude, while others had more consistent fatigue lives. This response was compared to other mechanical properties, in search of correlations. The wide scatter in baseline dwell fatigue life was observed only for material conditions resistant to stress relaxation. For selected materials and conditions, additional tests were then performed with the dwells shifted in part or in total to minimum tensile load. The tests performed with dwells at minimum load exhibited lower fatigue lives than max dwell tests, and also exhibited early crack initiation and a substantial increase in the number of initiation sites. These results could be explained in part by modeling evolution of peak stresses in the notch with continued dwell fatigue cycling. Fatigue-environment interactions were determined to limit life for the fatigue cycles with dwells.

15. SUBJECT TERMS
Heat resistant alloys; Turbine wheels; Fatigue (materials)

16. SECURITY CLASSIFICATION OF:			17. LIMITATION OF ABSTRACT	18. NUMBER OF PAGES	19a. NAME OF RESPONSIBLE PERSON STI Help Desk (email:help@sti.nasa.gov)
a. REPORT U	b. ABSTRACT U	c. THIS PAGE U	UU	53	19b. TELEPHONE NUMBER (include area code) 443-757-5802